RSC Advances

PAPER

View Article Online
View Journal | View Issue

Cite this: *RSC Adv.*, 2026, **16**, 14135

Sustainable mechanochemical activation of rock phosphate with oxalic acid for high-efficiency phosphorus fertilizers

Sanduni Dabare, [a] Imalka Munaweera *[a] and Saranga Diyabalanage [b]

Inefficient phosphorus fertilizer uses and increasing resource scarcity highlight the need for sustainable alternatives to conventional soluble fertilizers. This study presents a green mechanochemical strategy using biodegradable oxalic acid to activate Sri Lanka's Eppawala rock phosphate (ERP) and produce an efficient phosphorus fertilizer. The optimized formulation (OA-0.9) achieved 96–99% water-soluble phosphorus through the conversion of hydroxyapatite into monetite *via* calcium chelation and lattice disruption. Soil incubation studies showed sustained nutrient release, with 51.6% phosphorus released over 50 days compared with 13.6% from triple superphosphate (TSP), indicating reduced fixation in tropical soils. Agronomic trials demonstrated superior performance, producing 92.24 g fresh chili pods per plant, approximately 90% higher than TSP, with a germination index of 209.76%, suggesting phytostimulatory effects. Notably, a reduced application rate (50 kg ha^{-1}) achieved 79% of the maximum yield while improving phosphorus use efficiency by 58%. This environmentally benign approach valorizes the domestic phosphate resources, reduces fertilizer input requirements, and aligns nutrient release with crop demand. The findings demonstrate the potential of mechanochemical oxalic acid modification as a scalable strategy for producing sustainable, controlled-release phosphorus fertilizers that enhance agricultural productivity and resource efficiency.

Received 21st November 2025
Accepted 28th February 2026

DOI: 10.1039/d5ra09011c

rsc.li/rsc-advances

1 Introduction

Agriculture now stands at a crucial juncture worldwide. With the increasing population, the arable land per person is reducing, and therefore, the challenge to increase crop productivity with better resource-use efficiency has never been more pressing.[1] Within this context, phosphorus assumes a uniquely central role. One of the three primary macronutrients, phosphorus is integral to plant metabolism. It is a key structural constituent of nucleic acids and phospholipids, participating in energy transfer *via* ATP, which underpins growth, root development, and yield formation. Yet, despite its importance, phosphorus application in agriculture faces two inter-linked challenges: finite mineral resources and inefficient plant availability.[2]

Most inorganic phosphorus fertilizers are derived from mined rock phosphate (RP). Indeed, over 80% of global mined RP is used to manufacture phosphorus fertilisers.[3] However, there is growing concern that high-grade phosphate rock reserves will be economically depleted within the next half-century to century.[4,5] In the meantime, much of the RP available is the so-called "slow" rock phosphate form, essentially apatite minerals which are sparingly soluble and thus poorly available to plants in the short term. Studies report that untreated RP often releases only a small fraction of its P into solution over the course of a cropping season, meaning that it falls short of meeting crop demand without enhancement.[6] Mechanistically, this is because the calcium-apatite lattice in RP is thermodynamically stable, and dissolution under typical soil conditions is very slow. Together, these issues emphasize the urgent need for technologies that serve both to extend the useful lifespan of phosphate resources and increase the agronomic efficiency of P fertilisers.[7]

One promising pathway is the mechanochemical activation of RP. In this process, mechanical energy is used to refine the particle size, disrupt the crystal lattice, introduce defects, and increase surface area-all of which render the RP more reactive.[4] In effect, mechanochemical treatment transforms low-grade or slow-acting RP into more labile P sources, without the need for intensive chemical reagents or high temperatures.[8] Recent research has illustrated that mechanochemically treated RP can show substantially improved phosphorus solubility compared to untreated RP. This opens the way to more cost-effective and lower-impact fertilizer solutions.[9]

Another enhancement in the release of P, complementary to that produced by mechanical activation, is provided by organic acid modification.[10] Organic acids with low molecular weights (such as citric, malic, and oxalic acid) can exhibit high chelating

[a]*Department of Chemistry, Faculty of Applied Sciences, University of Sri Jayewardenepura, Nugegoda 10250, Sri Lanka. E-mail: imalka@sjp.ac.lk*
[b]*Instrument Center, Faculty of Applied Sciences, University of Sri Jayewardenepura, Nugegoda 10250, Sri Lanka*

ability, *i.e.*, they can bind and remove Ca^{2+} (or other metal ions) associated with apatite structures, thereby liberating phosphate ions into more soluble forms.[8] For example, mechanochemically activated RP treated with oxalic acid has been reported to release substantially higher P_2O_5 than untreated RP. The use of oxalic acid is especially appealing because it is biodegradable, less hazardous than many mineral acids, and aligns with the principles of green chemistry, reducing hazardous reagents, minimizing waste, and promoting benign processing.[11]

Eppawala rock phosphate (ERP) is an especially promising local resource in the context of Sri Lanka. Located in the North Central Province, ERP is the country's main domestic phosphate rock deposit and has been highlighted as an underused asset for the national fertiliser program. As with many rock phosphates, however, agronomic effectiveness is constrained by inherently low water solubility and a slow-release rate of P under field conditions. Activating ERP more effectively could thus unlock a home-grown phosphate fertilizer-reducing reliance on imported soluble P fertilizers and enhancing national food security.

From a sustainability and circular economy perspective, this research contributes to multiple goals.[12] The mechanochemical-organic acid approach uses primarily mechanical energy and mild organic acids, reducing chemical hazards and resource consumption while valorizing a low-grade domestic mineral resource.[13] Enhanced phosphorus availability allows for lower application rates, improving nutrient-use efficiency and reducing environmental losses such as runoff or soil fixation.[14] By leveraging local resources, promoting eco-friendly processing, and increasing agronomic efficiency, the approach exemplifies circular economy principles, converting natural materials into high-value fertilizers while minimizing environmental impact. Furthermore, effective phosphorus fertilization directly supports Sustainable Development Goal 2 (Zero Hunger), ensuring crop nutrition, yield stability, and long-term food security.[15] This work, therefore, integrates mineral chemistry, green chemistry, and sustainable agriculture into a coherent strategy for resource-efficient, environmentally responsible fertilizer production.

2 Methodology

2.1 Materials and chemicals

All reagents and chemicals, including oxalic acid, sulfuric acid, ascorbic acid, potassium dihydrogen phosphate, antimony potassium tartrate, ammonium molybdate, sodium acetate, acetic acid, Eriochrome Cyanine R, sodium hydroxide, hydrochloric acid, nitric acid, 1,10-phenanthroline monohydrate, hydroxylamine hydrochloride, iron(II) ammonium sulfate, sodium bicarbonate, and ERP, were used in this study. All analytical-grade reagents were purchased from Sigma-Aldrich (USA), while ERP was obtained locally.

2.2 Develop the oxalic acid-modified ERP (OA-ERP) using mechanochemical grinding

The ERP sample was thoroughly mixed with oxalic acid (OA) at various ERP-to-OA ratios (Table 1), followed by the addition of 5 mL of deionized water. The resulting mixture was then manually ground using a mortar and pestle for 1 hour. Prior to chemical analysis, the mixture was air-dried at 60 °C and ground to pass through a 1 mm sieve.

Table 1 Experimental design for preparing OA-ERP

Sample name	Mass of ERP (g)	Mass of oxalic acid (g)
OA – 0.2	10.00	2.00
OA – 0.6	10.00	6.00
OA – 0.9	10.00	9.00
OA – 1.0	10.00	10.00
OA – 1.2	10.00	12.00

The control-OA sample was prepared by mixing 10 g of ERP with 12 g of OA, followed by the addition of 5 mL of deionized water. The mixture was stirred for 1 hour without applying any mechanical treatment and subsequently dried at 60 °C.

2.3 Characterizations of ERP and OA-ERP

The structural, functional, and morphological characteristics of ERP, TSP, and OA-ERP were examined using X-ray diffraction (XRD), Fourier transform infrared (FTIR) spectroscopy, and scanning electron microscopy (SEM) coupled with energy dispersive X-ray spectrometry (EDX). XRD analysis was performed using a Rigaku Ultima IV diffractometer with Cu Kα radiation ($\lambda = 0.1537$ nm), operated at 40 kV and 30 mA, over a 2θ range of 10–60°, to evaluate crystallinity and phase composition. FTIR spectroscopy (Bruker Vertex 80) was employed to identify surface functional groups, where powdered samples were scanned in the 4000–400 cm^{-1} range using KBr pellets at a 4 cm^{-1} resolution. SEM (ZEISS model) was utilized to study surface morphology and particle structure, with samples mounted on copper stubs using carbon tape, reinforced with industrial adhesive, and sputter-coated with a thin gold–palladium layer for 30 seconds under vacuum. EDX analysis accompanied SEM observations to determine the elemental distribution and composition across the sample surface. Elemental composition was determined using an energy-dispersive X-ray fluorescence (EDXRF) spectrometer (Rigaku NEX CG, Rigaku Corporation, Tokyo, Japan).

2.4 Solubility, total and available phosphorus, and aluminium analysis of OA-ERP, ERP, and TSP

The total and available phosphorus (P) contents of ERP, OA-ERP, and TSP were determined using a UV-VIS spectrophotometer at a wavelength of 880 nm, following the development of a blue color based on the molybdenum blue method.[6] For color development, acid molybdate (Reagent A) and ascorbic acid (Reagent B) solutions were prepared. The acid molybdate reagent (Reagent A) consisted of 2.5 M H_2SO_4 containing 33 mM ammonium molybdate and 8.3 mM potassium antimony tartrate. The reducing solution (Reagent B) contained 0.10 M ascorbic acid prepared freshly prior to analysis. A 100 ppm standard phosphorus solution was prepared using potassium

dihydrogen phosphate (KH_2PO_4) and subsequently diluted to obtain working standards in the range of 0–8 ppm.

The solubility of OA-ERP at different pH levels was assessed by mixing 1 g of OA-ERP with 25 mL of water, with the pH adjusted using 0.1 M NaOH and 0.1 M HCl solutions. The mixture was stirred at 400 rpm for 24 hours, and the pH was then measured. Solubility values were determined using a UV-Vis spectrophotometer at 880 nm, employing the molybdenum blue method.[6]

About 4.00 g each of OA-ERP, control, and TSP were mixed with 100 mL of distilled water (pH = 7) as per SI 1996 No. 1342. Aliquots were collected at different time intervals, and after each withdrawal, the removed volume was replaced with fresh distilled water to maintain a constant total volume. The phosphorus content was determined using the molybdenum blue method with a UV-Vis spectrophotometer at 880 nm. Aluminium (Al) was determined using the 3500-Al B Eriochrome Cyanine R (ECR) method with a UV-Vis spectrophotometer by measuring the absorbance of the aluminium-ECR complex at 535 nm. Iron (Fe) content was also measured using a UV-Vis spectrophotometer at 470 nm. Residual/free oxalic acid present in OA-ERP formulations was quantified using a redox-based UV-Vis spectrophotometric method based on the reduction of potassium permanganate under acidic conditions. An aliquot of 0.375 mL of the extract was transferred into a reaction tube, followed by the addition of 1.875 mL of 2 N H_2SO_4 and 0.75 mL of 0.0015 M potassium permanganate solution. The mixture was vortexed and incubated for 10 min at room temperature to allow completion of the redox reaction between oxalic acid and permanganate. Absorbance was measured at 528 nm using a UV-Vis spectrophotometer. Oxalic acid concentration was determined using an external calibration curve prepared from analytical-grade oxalic acid standards and expressed as mg oxalic acid per g of fertilizer. All measurements were conducted in triplicate and reported as mean values.[16]

2.5 Soil characterization

Soil samples were air-dried at room temperature, gently disaggregated, and sieved to pass through a 2 mm mesh prior to analysis. Soil pH (ISO 10390:2005), bulk density, electrical conductivity, and water-holding capacity[17] were determined. Total soil P, Fe, and Al were extracted using aqua regia, prepared by mixing concentrated HCl and HNO_3 in a 3:1 ratio. Briefly, 2 g of soil was placed in a 250 mL conical flask, 20 mL of aqua regia was added, and the mixture was heated until clear. The digest was filtered into a 100 mL volumetric flask, and the volume was adjusted with distilled water.[6]

2.6 Release behavior of phosphorus, aluminium, and iron from OA-ERP during soil incubation

An incubation experiment was conducted under laboratory conditions to investigate the release kinetics of phosphorus (P) and the associated behaviour of aluminium (Al) and iron (Fe) from OA-ERP in soil. The study comprised seven treatment combinations arranged in a completely randomized design (CRD) with three replications. Air-dried soil samples (25 g, <2 mm) were placed in 250 mL plastic containers with screw caps. OA-ERP was applied at a rate equivalent to 120 mg P kg^{-1} of soil, with commercial TSP serving as the reference standard. Soil samples were destructively collected after 1, 2, 4, 24, and 50 days of incubation. Available phosphorus was extracted with deionized water and analyzed using the molybdenum blue method with a UV-Vis spectrophotometer. Aluminium (Al) concentration was determined following the 3500-Al B Eriochrome Cyanine R method by measuring the absorbance of the Al-ECR complex at 535 nm, while iron (Fe) content was also quantified using UV-Vis spectrophotometry.

2.7 Assessment of OA-ERP phytotoxicity on chilli (*Capsicum annuum*) seeds using a laboratory germination test

The phytostimulant or phytotoxic potential of OA-ERP was evaluated using a germination bioassay with commercial chilli seeds. The procedure was adapted and modified based on previously reported methods.[18–21] Based on the results explained in Section 2.4, OA-0.9, OA-1.0, and OA-1.2 were selected for the germination test due to their low pH levels. The results obtained were compared to the negative control, which contained distilled water. Petri dishes with a diameter of 100 mm were disinfected with 70% alcohol and allowed to dry. Chilli seeds were washed with purified water and dried in an oven at 30 °C. A 1% (w/v) agar solution was prepared and sterilized. For each treatment, 20 mL of molten agar was transferred into a sterile container. Separately, an aqueous fertilizer extract was prepared by dispersing approximately 35.0 mg of fertilizer was measured and combined with 30 mL of deionized water, then stirred at 500 rpm for 24 hours. The concentration of phosphorus of the aqueous extract was measured by the molybdenum blue method. P concentration was 500 μM. Subsequently, 1 mL of the aqueous fertilizer extract was added to the 20 mL of molten agar and mixed thoroughly under continuous stirring to ensure homogeneity. The homogenized agar and fertilizer extract mixture was then poured into sterile Petri dishes and allowed to solidify. Fifteen seeds were then placed on the agar media. The entire experiment was conducted in three batches, each containing 15 seeds. The Petri dishes were incubated in darkness for 12 hours and in light for 12 hours, over a period of 14 days at a temperature of 25 °C ± 1. The incubation period will end when at least 65% of the seeds in the control sample have germinated and developed roots at least 20 mm long (according to OPPTS 850.4200 seed germination/root elongation toxicity test). Subsequently, germinated seeds were counted and recorded as G, while root length was measured and denoted as L. The results obtained were analyzed by determining the following indicators: the relative germination index of the seeds (RSG) (eqn (1))[18], the relative growth index of the roots (RRG) (eqn (2))[18], and the germination index (GI) (eqn (3))[18], utilizing the subsequent calculation formulas:

$$\mathrm{RSG}(\%) = \frac{\text{Number of germinated seeds(sample)}}{\text{Number of germinated seeds(control)}} \times 100 \quad (1)$$

$$\mathrm{RRG}(\%) = \frac{\text{Mean root length of germinated seeds(sample)}}{\text{Mean root length of germinated seeds(control)}} \times 100 \quad (2)$$

$$\mathrm{GI}(\%) = \mathrm{RSG} \times \mathrm{RRG} \times 100 \quad (3)$$

2.8 Effect of OA-ERP phosphorus fertilizer on growth and nutrient uptake of chilli (*Capsicum* sp.) under laboratory conditions

Chilli seeds (*Capsicum* sp., cultivar KA2) were surface-sterilized by soaking in 1% (v/v) sodium hypochlorite for 5 minutes, then thoroughly rinsed with deionized water. Seeds were sown directly into plastic pots (100 mL) filled with soil with known properties (Table 2). Each pot was prepared by thoroughly mixing soil with the phosphorus (P) fertiliser treatment (the OA-ERP P source) at the designated treatment rate (T_1–T_{12}). Six seeds were sown per pot and all seedlings were allowed to grow simultaneously. Growth parameters were recorded on an individual plant basis. Since all treatments were subjected to the same planting density, any potential competition effects were consistent across treatments and did not bias comparative analysis. Soil moisture was maintained at around 80% of the water-holding capacity by periodic irrigation to ensure uniform growth conditions.

Plants were grown for one month (30 days) from sowing. At the end of the growth period, before harvest, shoot length (from soil surface to apex) and root length (from root-shoot junction to tip) of each plant were measured using a metric ruler to the nearest 1 mm. Then all plants in each pot were harvested. The roots were gently washed to remove adhering soil, dry, and then the shoots and roots were separated. Each portion was dried in an oven at 60 °C until constant weight (constant weight was reached when two weighings 24 hours apart differed by less than 0.05 of the sample's mass). Plant dry weights per pot were recorded.

After drying, samples were ground to pass a 0.5 mm sieve. A subsample (~0.2 g) of ground tissue was weighed into boiling tubes. Samples were digested using concentrated HNO_3 and H_2O_2 through conventional hot-plate acid digestion until a clear solution was obtained.[22,23] The digest was diluted to 50 mL with de-ionised water and filtered using a 0.45 μm filter.

Phosphorus concentration was determined *via* the molybdenum blue method following standard protocols for plant tissue.[24] Calcium (Ca) and iron (Fe) concentrations were measured using atomic absorption spectroscopy (AAS), in line with standard plant tissue analysis of macro- and micronutrients. To avoid pseudo-replication, measurements from seedlings originating from the same pot were averaged, and pot means were used as independent biological replicates for statistical analysis.

Available phosphorus (Olsen-P) in soil samples was determined by extracting soil with 0.5 M $NaHCO_3$ solution (pH 8.5) at a 1 : 20 soil-to-solution ratio, followed by colorimetric determination using the molybdenum blue method and spectrophotometric measurement at 880 nm.

Table 2 Fertilizer treatments for plant bioassay and plant trial

Treatment	P Fertilizer	Dose (kg ha^{-1})
Control	ERP	100
T_1	OA – 0.2	100
T_2	OA – 0.2	50
T_3	OA – 0.6	100
T_4	OA – 0.6	50
T_5	OA – 0.9	100
T_6	OA – 0.9	50
T_7	OA – 1.0	100
T_8	OA – 1.0	50
T_9	OA – 1.2	100
T_{10}	OA – 1.2	50
T_{11}	TSP	100
T_{12}	TSP	50

2.9 Greenhouse pot experiment for evaluating phosphorus fertiliser treatments on chilli (*Capsicum* sp.) growth and yield

The pot experiment was carried out under greenhouse conditions at Athurugiriya, Sri Lanka. Plastic pots (5 L capacity) were filled with a homogenized growth medium consisting of topsoil, sand, and organic matter mixed in a 2 : 1 : 1 (v/v) ratio. Before transplanting, the medium was analyzed to determine its initial chemical properties, including pH and available phosphorus (P). Certified seedlings of the cultivar recommended by the Department of Agriculture, Sri Lanka (DOA), were raised in a nursery and transplanted at the 4–6 true-leaf stage (approximately 30 days after sowing), with one seedling per pot. All pots received a uniform basal application of nitrogen (N) and potassium (K) fertilizers at the Department of Agriculture (DOA)-recommended rates for chilli cultivation, ensuring that nutrients other than phosphorus (P) were non-limiting. Phosphorus fertilizer treatments served as the sole variable factor, with the sources and application rates (expressed as kg ha^{-1}) detailed in Table 2. (ERP was applied only at the higher application rate in this study. ERP is characterized by low water solubility and slow phosphorus release, making it unsuitable for meeting the immediate phosphorus requirements of short-duration crops such as chili). Each fertiliser treatment was thoroughly mixed into the potting medium prior to transplanting. The layout followed a CRD with six replicates per treatment. Plants were kept at ambient greenhouse temperatures (~25–30 °C), irrigated regularly to maintain soil moisture near field capacity and standard pest and disease management was applied uniformly across all treatments. At 16 weeks after transplanting, pods number and the fresh weight per plant were measured.

2.10 Statistical analysis

All statistical analyses were performed using Minitab 18 statistical software. Data are presented as mean ± standard error of the mean (SEM), and replication varied depending on the experiment. Laboratory-based physicochemical and analytical measurements were conducted in triplicate ($n = 3$). The seed germination test included 45 seeds per treatment ($n = 45$). In

the plant bioassay, the pot was considered the experimental unit, with four independent pots per treatment ($n = 4$); multiple seedlings measured within a pot were treated as subsamples and averaged prior to analysis. In the greenhouse plant trial, each plant grown in an individual pot was considered an independent experimental unit ($n = 6$ plants per treatment).

Prior to analysis, data were assessed for normality using the Anderson-Darling test and for homogeneity of variance using Levene's test. For normally distributed data with equal variances, one-way analysis of variance (ANOVA) was conducted to determine significant differences among treatments. When significant differences were detected ($p < 0.05$), Tukey's Honest Significant Difference (HSD) post-hoc test was performed for pairwise comparisons between treatment groups.

Statistical significance was set at $\alpha = 0.05$. In all figures, different letters indicate statistically significant differences between treatments, while treatments sharing the same letter are not significantly different from each other.

3 Results and discussion

3.1 Characterizations of ERP and OA-ERP

XRF analysis (Table SI.1) of ERP revealed that calcium was the dominant oxide, with CaO content of 57.9 ± 0.077 wt%, followed by P_2O_5 (15.7 ± 0.014 wt%) and Fe_2O_3 (10.7 ± 0.013 wt%). Other major components included SiO_2 (7.53 ± 0.014 wt%), Al_2O_3 (3.83 ± 0.012 wt%), TiO_2 (1.06 ± 0.008 wt%), Na_2O (1.01 ± 0.067 wt%), K_2O (0.0618 ± 0.003 wt%), while MgO and MnO were present in minor amounts Elements such as Sr, Ba, Zn, Cu, Ni, Pb, As and rare earth elements (Ce, La, Nd, and Gd) were recorded in trace quantities, consistent with the accessory mineral assemblage of ERP, whereas Cd was not detected. The composition indicates that ERP consists primarily of calcium phosphate along with silicate and minor trace impurities.

After mechanochemical treatment with oxalic acid, OA-ERP (Table SI.1) showed an increased CaO content of 77.2 ± 0.038 wt% and a reduced P_2O_5 content of 6.84 ± 0.007 wt%, indicating selective phosphate leaching and also reflecting a dilution of ERP by the added oxalic acid Fe_2O_3 showed a slight increase to 12.2 ± 0.012 wt%, while SiO_2 (1.26 ± 0.005 wt%), Al_2O_3 (1.15 ± 0.006 wt%), TiO_2, and other minor oxides decreased. Trace elements such as Sr, Ba, Ce, La, and Nd decreased, while Gd increased (0.103 ± 0.004 wt%). Toxic elements Pb and As remained minimal, and Cd was not detected. These results confirm that oxalic acid treatment enriched CaO and reduced silicate and phosphate in ERP. The XRF results revealed that OA-ERP showed higher CaO and lower P_2O_5, SiO_2, Al_2O_3, and other minor oxides compared to ERP. Similar to previous studies,[9] these changes can be attributed to the partial breakdown of phosphate and gangue minerals and selective leaching of loosely bound components during mechanochemical treatment. Additionally, structural disorder induced by oxalic acid treatment likely enhanced surface reactivity and caused redistribution of elements within the mineral matrix, affecting the apparent XRF composition without causing actual elemental loss.[9,10] Because XRF compositions are normalized to 100 wt%, the elevated CaO content in OA-ERP represents a relative enrichment caused by preferential dissolution and removal of phosphate and gangue minerals, rather than an actual increase in total calcium concentration.

Upon OA modification, particularly under mechanochemical treatment, apparent structural modifications are evident. As illustrated in Fig. 1(A), the emergence of new peaks attributed to whewellite, a calcium oxalate monohydrate ($CaC_2O_4 \cdot H_2O$), indicates active reaction between oxalic acid and calcium-bearing apatite phases. This observation agrees with the literature: treatment of apatite with oxalic acid yields predominantly whewellite, and apatite peaks vanish with reaction.[25]

$$Ca_{10}(PO_4)_6(OH)_{2(s)} + 4H_2C_2O_{4(aq)} \rightarrow 4CaC_2O_{4(s)} + 6CaHPO_{4(s)} + 2H_2O_{(l)}$$

The formation of monetite ($CaHPO_4$) also becomes increasingly prominent in OA-ERP samples, signifying the partial dissolution of apatite and reprecipitation of calcium phosphate phases.

Mechanochemical activation combined with OA treatment significantly affected the crystallite size of ERP (Table SI.2). The crystallite size decreased progressively from 92.21 nm (ERP) to 59.53 nm (OA-0.6), indicating that grinding induced crystal fragmentation and reduced crystallinity. The unit cell parameters displayed anisotropic changes: the *a*-axis initially expanded at low OA content (OA-0.2) due to oxalate incorporation but slightly contracted at higher OA content (OA-0.6), likely due to lattice strain. The *c*-axis consistently increased, reflecting expansion along the hexagonal channel where oxalate anions are accommodated. Mechanochemical activation not only facilitated oxalate substitution by enhancing particle contact but also introduced lattice defects, contributing to the observed size reduction and structural distortion.[11]

The addition of OA-0.2 and OA-0.6 samples further reveals the influence of oxalic acid amount. At lower oxalic acid ratios (OA-0.2), apatite peaks remain prominent (Fig. 1(B)(f)), but initial signs of whewellite, weddellite (calcium oxalate dihydrate ($Ca(C_2O_4) \cdot 2H_2O$)), and monetite formation are observed, suggesting limited but active interaction. OA-1.2 and control-OA show residual OA, emphasizing the excess amount of oxalic acid. As Fig. 1(A)(a) and (b) illustrates, as the oxalic acid content increases, the apatite peak intensity declines more significantly, reflecting a decrease in the crystallinity of the apatite phase, which gradually occurs. The gradual decline in crystallinity indicated an increase in P release from apatite.[26] According to the literature, ion exchange dissolution is the primary mechanism for apatite dissolution.[27–30] This model suggests that protons and acid anions from the solution adsorb onto the apatite surface,[28] leading to the release of calcium and phosphate ions into the solution.[18]

These structural transformations observed by XRD were corroborated by SEM micrographs, which revealed corresponding morphological evolution. SEM images revealed distinct morphological transformations of rock phosphate with increasing oxalic acid content. In the OA-0.2 sample (Fig. 2(F)), well-defined hexagonal crystal shapes characteristic of apatite were clearly visible, indicating that the apatite phase remained

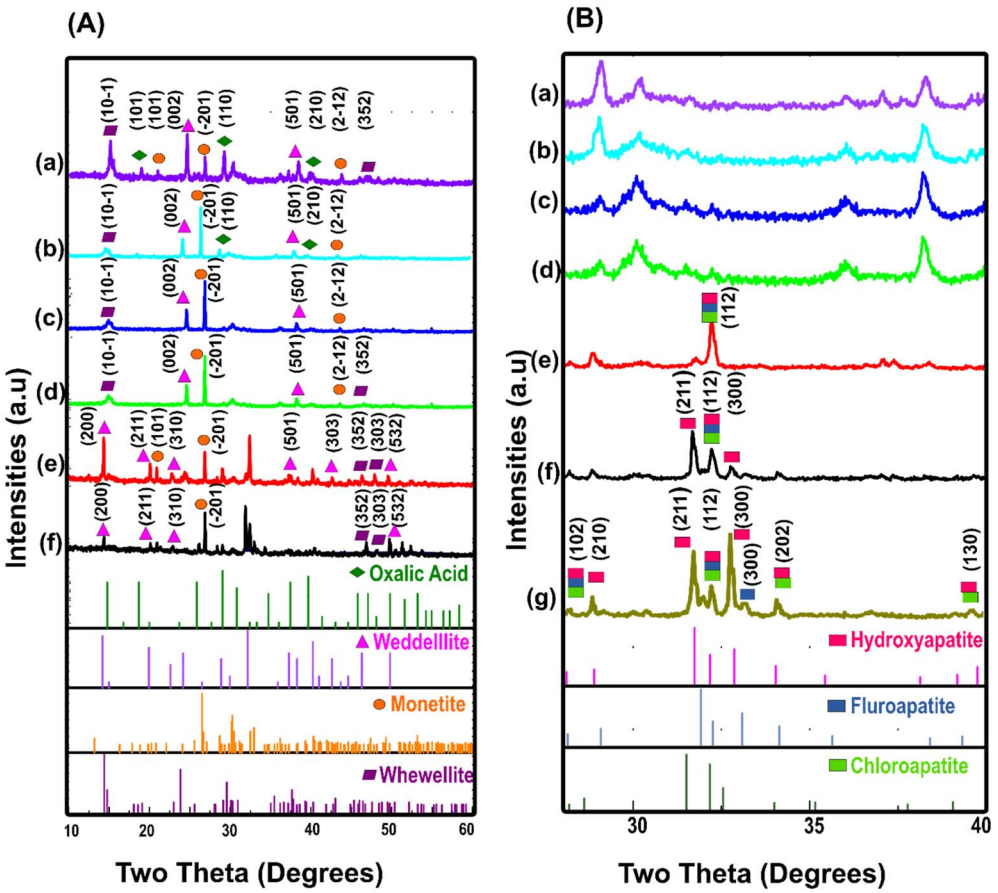

Fig. 1 (A) PXRD pattern of (a) control-OA, (b) OA-1.2, (c) OA-1.0 (d) OA-0.9 (e) OA-0.6 (f) OA-0.2 sample, matching with, oxalic acid, whewellite, weddellite and monetite (JCPDS card No. 01-071-1759) (B) Apatite peak of OA-ERP (a) control-OA, (b) OA-1.2, (c) OA-1.0 (d) OA-0.9 (e) OA-0.6 (f) OA-0.2 and (g) ERP matching with hydroxyapatite (JCPDS Card No. 01-072-1243), chlorapatite (JCPDS Card No. 01-073-1728), fluorapatite (JCPDS Card No. 01-073-1727).

largely intact with only limited surface dissolution. At this low acid ratio, oxalic acid likely caused mild etching at crystal edges without significant lattice disruption, preserving the original hexagonal habit of the apatite grains.

In the OA-0.6 sample, the hexagonal outlines were still discernible but became partially distorted and roughened, suggesting partial dissolution of the apatite surface and the onset of secondary phase formation (Fig. 2(E). By OA-0.9, the hexagonal morphology was barely visible, indicating more extensive reaction between oxalic acid and the apatite mineral, which led to the breakdown of the crystalline structure (Fig. 2(D).[31]

At higher oxalic acid ratios (OA-1.0 and OA-1.2), the hexagonal morphology disappeared entirely, and the particles exhibited plate-like or flaky morphologies Fig. 2(B) and (C). These plates are consistent with the formation of monetite ($CaHPO_4$) and/or calcium oxalate phases, which typically crystallize as thin, irregular plates or tabular structures. The progressive loss of hexagonal features and emergence of plate-like textures reflect the increasing degree of apatite dissolution and reprecipitation of new, more soluble phases.[32,33]

The SEM images of the pristine ERP (Fig. 2(G) reveal a heterogeneous and compact morphology, consisting predominantly of irregularly shaped, coarse aggregates with rough and uneven surfaces. Well-defined hexagonal prismatic crystals are not apparent, suggesting that crystal boundaries are closely intergrown or covered by fine mineral particles. This irregular morphology is typical for natural apatite-rich rock phosphates, where fluorapatite, chlorapatite, and hydroxyapatite phases coexist with minor impurities and secondary minerals formed during geological weathering.[34]

The application of OA to ERP, even in the absence of intensive mechanochemical grinding, induces notable structural and morphological changes in the apatite lattice. These changes can be explained by the unique chemical interactions between OA, a weak organic acid, and the surface of the apatite mineral.

Oxalic acid, being a dicarboxylic organic acid, exhibits a strong chelating affinity for calcium ions. When applied to ERP, OA preferentially binds to surface-exposed calcium sites on the apatite crystals. This interaction destabilizes the local lattice environment, effectively weakening the electrostatic network that stabilizes the calcium-phosphate framework.[9,11] The selective chelation of calcium promotes partial dissolution of the lattice, releasing phosphate into the surrounding medium. Unlike strong mineral acids, OA operates gradually, allowing surface-limited modifications rather than complete

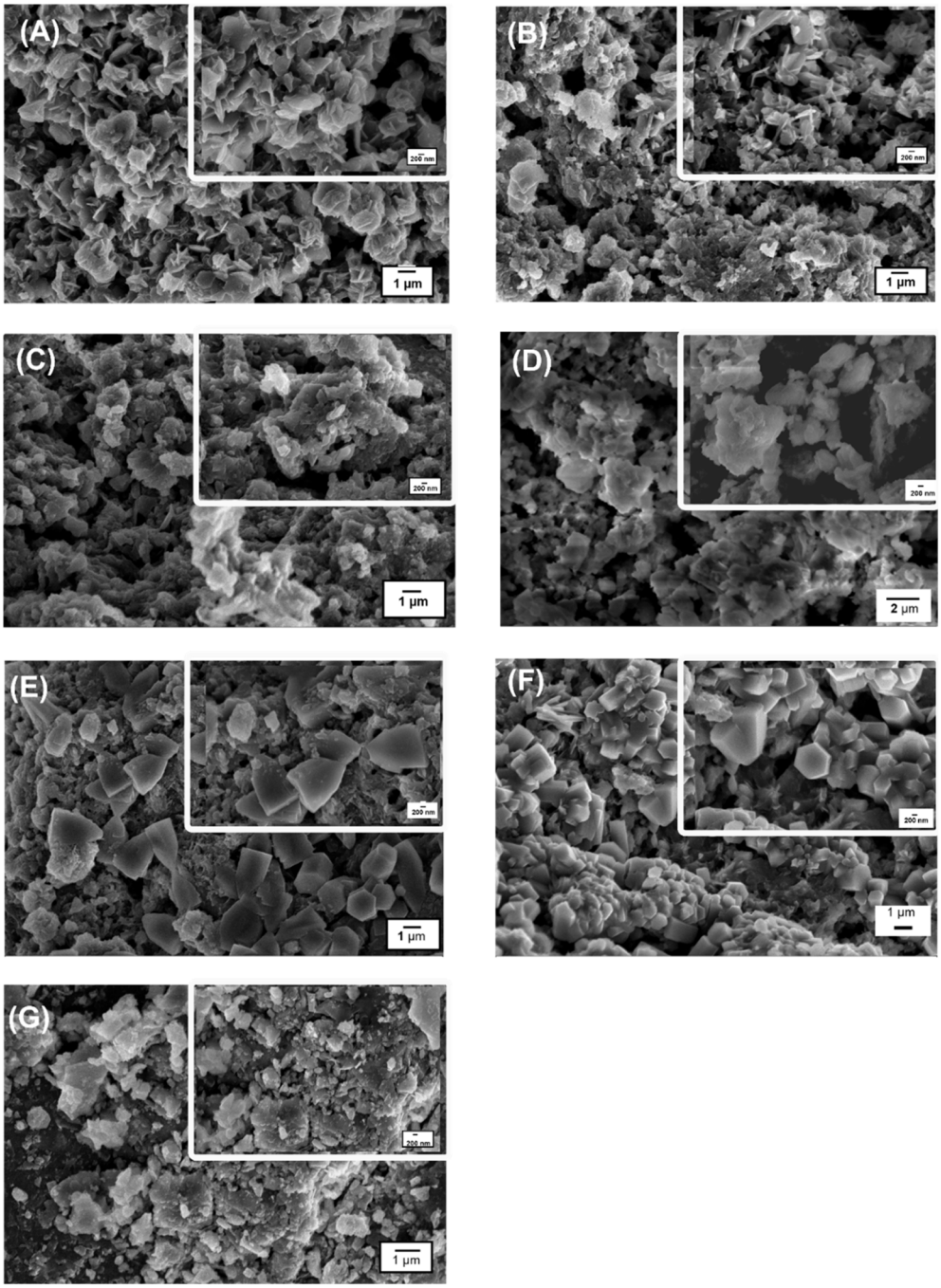

Fig. 2 SEM morphology of OA-ERP (A) control-OA, (B) OA-1.2, (C) OA-1.0 (D) OA-0.9 (E) OA-0.6 (F) OA-0.2 and (G) ERP (Panel D was acquired at 2 μm magnification to better resolve surface morphology; all other panels are at 1 μm magnification).

breakdown of the bulk mineral structure, which is consistent with observations of morphological roughening rather than wholesale disintegration.[10]

Concomitant with lattice disruption, the released calcium ions readily react with excess oxalate ions to form secondary calcium-containing phases. Predominantly, these include calcium oxalate ($CaC_2O_4 \cdot xH_2O$) and, under slightly acidic or low-water conditions, monetite ($CaHPO_4$). The formation of these secondary phases occurs on the mineral surface or in close proximity, contributing to the observed precipitation features and surface coatings. These secondary phases can locally modify the microstructure and influence the solubility and reactivity of the remaining apatite.[9]

From a morphological perspective, the combined effect of surface calcium chelation, partial lattice dissolution, and secondary phase formation results in the etching, pitting, and roughening of apatite crystals observed in SEM and XRD analyses. Such structural modifications not only alter the physical

appearance but also enhance the accessibility of phosphate ions, providing a plausible explanation for the improved extractability and bioavailability of phosphorus in subsequent soil incubation experiments.

Despite the absence of distinct crystal faces in SEM, the sharp diffraction peaks in the XRD pattern confirm that the ERP possesses a highly crystalline apatite structure. The contrast between the SEM and XRD observations indicates that, although the particles exhibit irregular external morphology, their internal lattice structure remains well ordered. The compact and dense morphology is consistent with the low surface reactivity and limited phosphorus solubility characteristic of unmodified RP These features provide a reference baseline for assessing the surface transformations observed in the OA-modified ERP samples.

In the ERP, the FTIR spectrum (Fig. 3), the bands observed at approximately 1038, 602, and 466 cm^{-1} are corresponding to the ν_3 asymmetric stretching, ν_4 bending, and ν_2 bending modes of the PO_4^{3-} groups, confirming the presence of phosphate in the structures.[35–37]

The sharp absorption band of about 3445 cm^{-1} results from OH stretching. Additionally, the distinct sharp band at 1384 cm^{-1} corresponds to the anti-symmetric stretching of C=O, highlighting the presence of carbonyl functional groups. Almost similar data were found in other literature.[38–40]

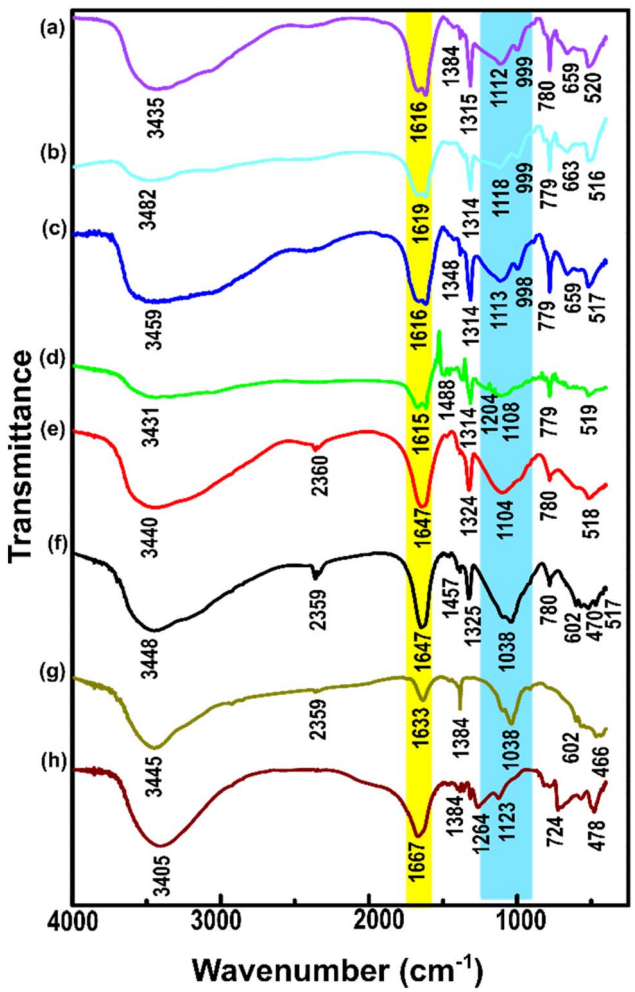

Fig. 3 FTIR analysis of (a) control-OA, (b) OA-1.2, (c) OA-1.0 (d) OA-0.9 (e) OA-0.6, (f) OA-0.2, (g) ERP and (h) oxalic acid.

The FTIR spectra of the OA-ERP samples exhibit pronounced absorptions corresponding to the asymmetric and symmetric stretching vibrations of the PO_4^{3-} groups. Compared with the unmodified ERP, the OA-ERP spectra show noticeable shifts and intensity variations, indicating structural modification of the phosphate environment. New absorption bands observed at 1162 and 1108 cm^{-1} in the OA-0.9 sample are also attributed to the PO_4^{3-} stretching vibrations, suggesting alterations in the local bonding environment of the phosphate tetrahedra.[41]

A progressive broadening is observed within the asymmetric stretching region (~1030–1120 cm^{-1}), with characteristic PO_4^{3-} bands appearing at 1038, 1104, 1108, 1113, 1118, and 1112 cm^{-1} for OA-0.2, OA-0.6, OA-0.9, OA-1.0, OA-1.2, and OA-control samples, respectively. This spectral broadening and slight band shifting reflect increased structural disorder in the phosphate lattice, possibly caused by the incorporation of oxalate or other anionic species into the apatite framework. Such substitutions perturb the PO_4^{3-} vibrational symmetry and induce local distortions within the apatite unit cell (blue-shaded region in Fig. 3(B)).[27]

The observed shifts and broadening of the phosphate (PO_4^{3-}) bands in OA-modified ERP can be attributed to chemical interactions between oxalic acid and the apatite lattice. During modification, oxalate anions ($C_2O_4^{2-}$) can partially substitute for phosphate (PO_4^{3-}) or interact with surface calcium ions (Ca^{2+}) through ion-exchange and complexation mechanisms. This interaction perturbs the local symmetry of the phosphate tetrahedra, resulting in changes in the vibrational energy and hence the FTIR band positions.

Apatite lattice: $Ca_{10}(PO_4)_6(F, Cl, OH)_2 + C_2O_4^{2-} \rightarrow$ partially substituted lattice $Ca_{10}(PO_4)_{6-x}(C_2O_4)_x(F, Cl, OH)_2$ + Ca-oxalate surface complexes

Furthermore, oxalic acid can promote partial dissolution of the apatite structure, followed by reprecipitation of calcium oxalate (whewellite or weddellite) and calcium hydrogen phosphate (monetite) phases, as confirmed by XRD.

$$Ca_{10}(PO_4)_6(F, Cl, OH)_2 + nH_2C_2O_4 \rightarrow \text{dissolved } Ca^{2+}, PO_4^{3-} \text{ species, and residual lattice}$$

$$Ca^{2+} + C_2O_4^{2-} \rightarrow CaC_2O_4 \text{ (whewellite/weddellite)}$$

$$Ca^{2+} + HPO_4^{2-} \rightarrow CaHPO_4 \text{ (monetite)}$$

$$Ca_{10}(PO_4)_6(F, Cl, OH)_2 + H_2C_2O_4 \rightarrow \text{residual apatite} + CaC_2O_4 \text{ (whewellite/weddellite)} + CaHPO_4 \text{ (monetite)}$$

These newly formed phases and local lattice distortions lead to the observed broadening of the asymmetric stretching region (1030–1120 cm^{-1}). The simultaneous presence of crystalline and partially disordered domains, as evidenced by SEM, supports this

mechanism. Thus, the combined FTIR, XRD, and SEM results suggest that oxalic acid treatment induces structural reorganization within the apatite lattice, increasing the chemical reactivity and potential phosphorus release of the modified ERP.

With broadening, absorption bands associated with the P–O–H stretching vibrations are observed at 998 and 999 cm^{-1} in OA-1.0 and OA-1.2, further confirming monetite ($CaHPO_4$) formation. Additional bands in the 466–602 cm^{-1} region correspond to bending vibrations of O–P–O and P–O–Ca linkages, characteristic of phosphate frameworks.[41]

Bands associated with O–C–O bending vibrations were observed at 779–780 cm^{-1} in OA-ERP, and the intensity of this band increased with higher oxalic acid content, confirming the formation of calcium oxalate. The asymmetric stretching vibration (ν_{as}) of the COO^- group appeared at 1667 cm^{-1} in pure oxalic acid and shifted to 1647–1615 cm^{-1} in OA-ERP samples, while the symmetric stretching vibration (ν_s) of COO^- was observed at 1384 cm^{-1} in oxalic acid.[40] The broad, intense COO^- bands centered at 1615–1619 cm^{-1} in OA-ERP indicate coordination of Ca^{2+} ions through electrostatic attraction and/or ion-exchange interactions, forming surface complexes of the type ($R–COO^-\cdots Ca^{2+}$) (yellow region in Fig. 3(B)).[42]

$$R–COO^- + Ca–OH_{surface} \rightarrow (R–COO^-\cdots Ca^{2+})_{surface} + OH^-$$

Furthermore, the secondary carbonyl and metal-carboxylate stretching vibrations observed at 1325–1314 cm^{-1} further confirm the formation of calcium oxalate species resulting from the reaction between oxalic acid and rock phosphate.

EDX analysis confirmed the presence of significant amounts of calcium (Ca), phosphorus (P), oxygen (O), and carbon (C), with minor impurities of iron (Fe) and aluminum (Al), consistent with previous reports. The relative content of O and C increased in OA-ERP, particularly in OA-1.2, reflecting the incorporation of oxalate during activation (Fig. SI.1).

3.2 Water release study of OA-ERP and TSP

Fig. 4(A) compares the total phosphorus content and the proportion of water-soluble phosphorus (as a percentage of total phosphorus) in ERP, TSP, and OA-ERP at neutral pH for 1440 minutes. The results indicate that ERP contains the highest total phosphorus content (38.79 ± 1.50%) but an extremely low water-soluble fraction (0.001%), consistent with previous findings describing ERP as a phosphate source with poor immediate availability due to its insoluble mineral structure.[43–45] In contrast, TSP contains a comparable total phosphorus level (38.31%) but markedly higher solubility (91.69%), confirming its superior plant availability.

Among the OA-ERP samples, the total phosphorus content decreases with increasing OA concentration, from 31.56 ± 0.21% in OA-0.2 to 26.11 ± 0.99% in OA-0.6, followed by a slight increase at higher OA levels. This trend can be attributed to the partial dissolution of phosphate minerals at low OA concentrations, which reduces phosphorus in the residual solid phase. At higher OA loadings, reprecipitation or complexation with calcium oxalate likely occurs, resulting in a modest increase in phosphorus retention.[46,47]

In contrast, the water-soluble phosphorus content is markedly enhanced relative to unmodified ERP. At low OA treatment (OA-0.2), solubility reaches 38.83 ± 0.71%, while at higher OA concentrations (0.9–1.2) solubility dramatically increases to 96–99%, approaching or even exceeding that of TSP. This significant improvement is attributed to the dissolution of apatite by oxalic acid, which releases phosphate into solution, while the concurrent formation of calcium oxalate precipitate concurrently reduces free Ca^{2+} activity, further enhancing phosphorus solubility.[46,47]

The phosphate dissolution behaviour of OA-ERP exhibits a strong dependence on both the pH and the oxalic acid treatment level (Fig. 4(B). Under highly acidic conditions (pH 2.5–5.5), all OA-modified samples showed substantially greater P release compared to neutral and alkaline conditions, reflecting the increased solubility of calcium phosphates under acidic

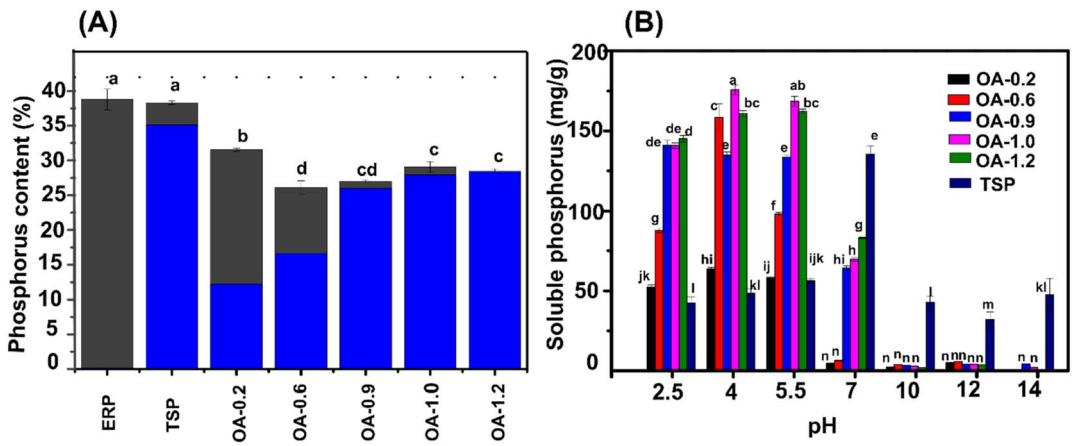

Fig. 4 (A) Total phosphorus content (black colour bar) and water-soluble phosphorus fraction (from total phosphorus) (blue colour bar) of ERP, TSP, and OA-ERP. (B) Soluble phosphorus content of OA-ERP across different pH levels (2.5–14) for 1440 minutes. Different letters indicate statistically significant differences between groups (Tukey's HSD test, $p < 0.05$) ($n = 3$).

environments. Notably, at pH 2.5, increasing the oxalic acid ratio from 0.2 to 1.2 progressive raise P release from 52.6 ± 1.2 mg L^{-1} (OA-0.2) to 145.1 ± 2.1 mg L^{-1} (OA-1.2), indicating that higher oxalic acid treatment effectively enhances surface modification and formation of soluble calcium–oxalate–phosphate complexes. At pH 4 and 5.5, a similar trend is observed, with OA-0.6 and OA-1.0 showing the highest P release, suggesting an optimal oxalic acid ratio for solubility enhancement at moderately acidic conditions.

In comparison, TSP exhibits near-complete solubility across all tested pH levels, with phosphorus release consistently above 90%, reflecting its inherently high immediate plant availability.[48] These findings indicate that while TSP provides rapid P availability regardless of pH, OA- ERP can achieve comparable solubility under acidic conditions, and its solubility can be fine-tuned *via* oxalic acid treatment, offering a phosphorus release advantage in soils with variable pH.[49,50]

In contrast, at near-neutral and alkaline pH (7–14), phosphate release drastically decreased across all samples, consistent with the lower solubility of calcium phosphates in basic conditions (Fig. 4(B)). Interestingly, the P release for higher oxalic acid treatments (OA-0.9 to OA-1.2) at pH 7 remained significantly higher (64–83 mg L^{-1}) than that of lower treatments (OA-0.2 and OA-0.6, 4–6 mg L^{-1}), indicating that oxalic acid modification partially mitigates the surface passivation effects of calcium phosphate and enhances dissolution even under less favourable conditions. At very high pH (10–14), P release for all samples approaches minimal levels (<6 mg L^{-1}), suggesting strong surface passivation and precipitation of less soluble calcium-phosphate and calcium-oxalate phases. Apatite dissolution at alkaline pH is inherently limited. According to the literature, in the pH range of 4.5–8.2, hydroxyapatite exhibits incongruent dissolution, yielding a solution with a high Ca/P ratio. At pH values above 8.2, dissolution becomes almost negligible, and the solution shows very low Ca/P ratios. This

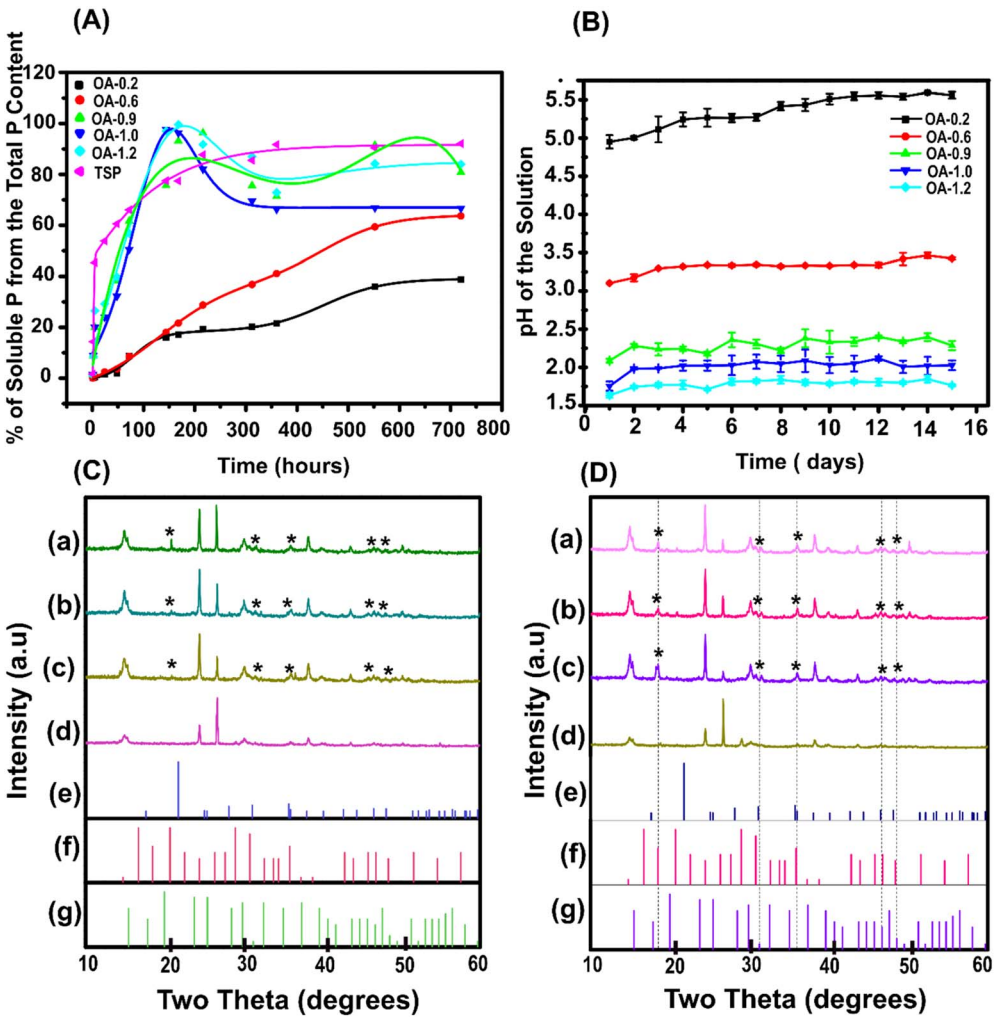

Fig. 5 (A) Water (pH = 7) releases the percentage of phosphorus from the total phosphorus content of OA-ERP and TSP over time (hours) (n = 3), (B) change in pH of the medium (water) over time during water release of OA-ERP (n = 3), (C) PXRD of the residue of OA-0.9 after water release (a) after 15 days (b) after 10 days (c) after 4 days (d) initial (e) iron phosphate JCPDS No: 01-072-1161 (f) aluminium iron phosphate hydrate JPCDS No: 00-002-0149 (g) iron phosphate JPCDS No: 00-019-0638 (C) PXRD of the residue of OA-1.2 after water release (a) after 15 days (b) after 10 days (c) after 4 days (d) initial (e) iron phosphate JCPDS No: 01-072-1161 (f) aluminium iron phosphate hydrate JPCDS No: 00-002-0149 (g) iron phosphate JPCDS No: 00-019-0638 (* formation of iron phosphate/aluminium iron phosphate).

behaviour is partly attributed to the formation of a negatively charged surface on calcium-deficient hydroxyapatite (CDHA), which promotes re-adsorption of calcium ions and desorption of phosphate ions. Surface charge plays a crucial role: at alkaline pH, apatite surfaces are negatively charged, proton adsorption is minimal, and the catalytic effect of protons in weakening Ca–O bonds is greatly reduced.[31,51,52]

As illustrated in Fig. 5(A), at pH 7, OA-ERP exhibited a rapid initial phosphate release during the first 48 hours, reaching approximately 20% of the total P content. Within six days, the soluble P fraction approached ~99% of the total P content. In several treatments, transient declines or oscillations were observed in the release curves, attributed to secondary precipitation of $AlPO_4$ and $FePO_4$, as confirmed by XRD analysis shows in Fig. 5(C) and (D) at 10 and 15 days. Following the initial phase, a diffusion-controlled stage dominated P release behaviour, consistent with classical apatite dissolution kinetics.

The amount of oxalic acid used in ERP modification strongly influenced the pH evolution of the medium (Fig. 5(B)). For OA-1.2, the initial water pH of 7 dropped sharply to 1.5 and remained nearly constant throughout the experiment, while OA-1.0 reduced pH to ~2. Lower oxalic acid treatments (OA-0.6 and OA-0.2) resulted in more moderate drops, to 3.5 and 5, respectively. This acidification plays a crucial role in controlling phosphate release, enhancing solubility while simultaneously promoting the formation of secondary precipitates that influence overall release kinetics.

Phosphate readily complexes with several cations, with affinity generally decreasing in the order $Al^{3+} > Fe^{2+} > Mg^{2+} > Cu^{2+} > Zn^{2+}$.[39] Under acidic conditions, Al^{3+} and Fe^{2+} are the particularly significant. Al^{3+} form stronger complexes with oxalate than with phosphate, explaining its relatively lower phosphate release at later stages.[53] In contrast, Fe^{2+} readily precipitates as $FePO_4$ at pH 1–3. The low solubility product constants (K_{sp}) of $AlPO_4$ (9.84×10^{-21}) and $FePO_4$ [or $Fe_2(PO_4)_3$] (9.91×10^{-16}) make these phases thermodynamically stable under acidic conditions, thereby reducing soluble P through reprecipitation.[54] The observed declines in P release following the initial dissolution phase are thus consistent with the formation of $AlPO_4$ and $FePO_4$ (ref. 3 and 38) particularly in treatments with stronger acidification (OA-1.0 and OA-1.2).

OA-ERP contains calcium hydrogen phosphate ($CaHPO_4$) as one of its major phases. Its dissolution initially releases phosphate but also elevates Ca^{2+} concentrations near particle surfaces.

$$CaHPO_{4(s)} \leftrightarrow {Ca^{2+}}_{(aq)} + {HPO_4}^{2-}{}_{(aq)}$$

At a typical environmental pH, the hydrogen phosphate anion is in acid–base equilibrium:

$${HPO_4}^{2-}{}_{(aq)} \leftrightarrow {H^+}_{(aq)} + {PO_4}^{3-}{}_{(aq)}$$

Therefore, dissolution supplies both Ca^{2+} and (after deprotonation) ${PO_4}^{3-}$ to local solution. When the local Ca/P ratio becomes sufficiently high, precipitation of Ca-rich phases layers form, further slowing P release.

$$10{Ca^{2+}}_{(aq)} + 6{PO_4}^{3-}{}_{(aq)} + 2{OH^-}_{(aq)} \rightarrow Ca_{10}(PO_4)_6(OH)_{2(s)}$$

Precipitation can occur *via* intermediate, more hydrated phase like octacalcium phosphate which then transform to apatite, producing a more Ca rich, less soluble surface layer.

$$8{Ca^{2+}}_{(aq)} + 2{HPO_4}^{2-}{}_{(aq)} + 4{PO_4}^{3-} + 5{H_2O}_{(l)} \rightarrow Ca_8(HPO_4)_2(PO_4)_4{\cdot}5H_2O_{(s)}$$

Octacalcium phosphate has a Ca/P ratio≈ of 1.33 and can subsequently recrystallize to hydroxyapatite as conditions evolve (loss of structural water/proton transfer), producing a more Ca-rich, less soluble apatite surface layer.[31,55–57]

Free (unprecipitated) oxalate moderates P release by two complementary pathways: (1) it complexes or precipitates Ca^{2+} in solution as CaC_2O_4, thereby lowering the activity of free Ca^{2+} available for apatite formation; and (2) it adsorbs/chelates Ca at particle surfaces (surface complexation), which disrupts or competes with Ca–PO_4 bonding required for forming a passivating apatite layer. Both effects reduce the local Ca/P ratio at the particle–solution interface, thereby suppressing apatite-type precipitation (Ca/P ≈ 1.67) and re-enhancing phosphate dissolution. Note that oxalate speciation ($H_2C_2O_4 \rightleftharpoons HC_2O_4^- \rightleftharpoons {C_2O_4}^{2-}$) is pH dependent ($pK_{a_1} \approx 1.3$, $pK_{a_2} \approx 4.3$), so the efficiency of these pathways varies with solution pH; at very low pH, less ${C_2O_4}^{2-}$ is available for complexation/precipitation.

Calcium oxalate precipitation (consuming free oxatale and Ca^{2+})

$${Ca^{2+}}_{(aq)} + {C_2O_4}^{2-}{}_{(aq)} \leftrightarrow CaC_2O_{4(s)}$$

Surface complexation/absorption

$$\equiv\text{Surface-}Ca^{2+} + {C_2O_4}^{2-} \leftrightarrow \equiv\text{Surface-Ca–}C_2O_4^{(ads)}$$

$\equiv$Surface-Ca^{2+} represents a surface-associated Ca site

This process effectively sequesters surface Ca, weakens the integrity of a nascent Ca-rich passivating layer, and/or blocks further Ca-PO_4 bonding sites.

If oxalate removes a fraction f of the available Ca locally (either by precipitation or strong surface complexation), the effective local Ca/P ratio decreases according to:

$$Ca/P_{local,eff} = \frac{[Ca^{2+}]_{total}(1-f)}{[P]_{local}}$$

When the local Ca/P falls below the threshold for apatite precipitation (≈1.67), further apatite like passivation is suppressed, and dissolution of $CaHPO_4$ is promoted.[58–60]

The release dynamics of triple superphosphate (TSP) followed the Hill function, producing a characteristic sigmoidal release curve (Fig. 5(A)). This pattern reflects the rapid dissolution of monocalcium phosphate [$Ca(H_2PO_4)_2 \cdot H_2O$], the primary soluble phase in TSP, accounting for the sharp initial increase in solution P concentration. The subsequent plateau phase indicates equilibrium solubility, beyond which additional release is minimal. Such behavior underscores the highly soluble nature of TSP and its limited suitability as a controlled-release fertilizer, as P availability is largely confined to the initial dissolution phase rather than being sustained over time.

Comparable release profiles have been widely reported in soil and aqueous systems, where P from TSP is rapidly solubilized but readily reprecipitated or fixed with Al, Fe, or Ca, depending on soil pH.[61–63] For instance, a rapid burst of P release from TSP granules is typically followed by stabilization of solution concentrations within hours.[64] Roy *et al.* (2006)[65] similarly described TSP as a highly water-soluble source of P with minimal capacity for gradual nutrient release. This distinguish it from RP or modified phosphate fertilizers, which are designed for controlled release. TSP dissolution is nearly instantaneous compared to partially acidulated rock phosphates, which show extended release due to the presence of sparingly soluble Ca–P phases.[66]

In contrast, OA-ERP release data were best fitted to a bi-dose response model, also referred to as a dual-phase nutrient release model. This model captures (i) an initial rapid release from surface-bound and loosely associated phosphate fractions, followed by (ii) a slower, sustained phase governed by diffusion and re-precipitation dynamics, including Ca-rich layer formation and $AlPO_4$/$FePO_4$ precipitation. This biphasic release behaviour aligns with the "immediate and residual effect" concept commonly discussed for P fertilizers, in which a portion of the P is immediately available for plant uptake while another fraction is gradually released over time.

Similar dual-phase phosphorus (P) release patterns have been observed in various fertilizer systems. In partially acidulated rock phosphates (PARP), studies indicate an initial surge of loosely bound phosphate, followed by a slower, sustained release phase as sparingly soluble calcium-phosphate phases gradually dissolve. For example, one incubation study on PARP showed an increasing trend in water-soluble P in the early stages (7–14 days) followed by a notable reduction in later stages, consistent with a biphasic release pattern.[62,64] In fertilizers modified with organic acids such as oxalate or citrate, these organic amendments enhance phosphate release by complexing surface Ca^{2+} ions and preventing the formation of apatite-like passivation layers, thereby promoting a more gradual and extended release. Similarly, controlled-release phosphate fertilizers such as polymer-coated or chelator-assisted formulations exhibits characteristic biphasic behaviour, with an early phase to meet initial crop demand, followed by a secondary phase that sustains phosphorus availability over time.[67,68] Collectively, these findings suggest that a system which integrates these mechanisms such as OA-ERP effectively combines surface-bound phosphate desorption, organic acid-mediated modulation of Ca/P ratios, and controlled precipitation or dissolution of secondary mineral phases. This synergistic combination yields a sustained P supply profile that bridges the gap between highly soluble fertilizers like TSP and conventional slow-release formulations.

Hematite (Fe_2O_3) and Al_2O_3 are the main impurities contained in ERP. In an acidic environment, Fe^{2+} and Al^{3+} are released. Fe release and Al release from OA-ERP with time are illustrated in Fig. 6(D) and (E), respectively. For Fe, OA-1.2 released 19.99 mg g^{-1}, significantly higher than others. As described by Panias *et al.* (1996),[69] dissolution of Fe occurs through three stages: activation of the hematite surface, generation of ferrous ions, and an autocatalytic dissolution phase. Initially, oxalate adsorbs onto Fe(III) surface sites forming ≡Fe(III)–oxalate surface complexes. Electron transfer within this complex reduces Fe(III) to Fe(II), which is released into solution along with the oxidation of oxalate to CO_2. The liberated Fe(II) subsequently forms soluble Fe(II)-oxalate complexes such as $[Fe(C_2O_4)]^0$ or $[Fe(C_2O_4)_2]^{2-}$. These species enhance further Fe(III) reduction and dissolution, leading to autocatalytic release of Fe from the surface. As the concentration of Fe^{2+} increases, an autocatalytic dissolution process is initiated,

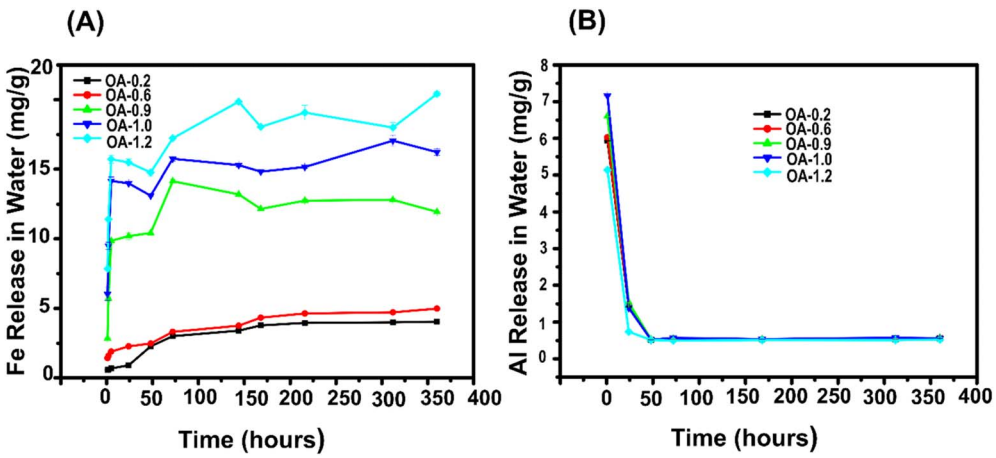

Fig. 6 (A) Fe release from OA-ERP in water (pH = 7) and (B) Al release from OA-ERP in water (pH = 7) (n = 3).

during which Fe^{2+} forms soluble Fe(II)-oxalate complexes. The initially rapid Fe release phase is attributed to the abundance of reactive surface sites and oxalate ligands, while the subsequent decline reflects site depletion and the stabilization of Fe as soluble Fe-oxalate complexes or surface-adsorbed species.[70]

Surface absorption and initial reaction

$$\equiv Fe^{3+}{}_{(surface)} + C_2O_4{}^{2-} \rightarrow \equiv Fe^{3+} - C_2O_4{}^{2-} \rightarrow Fe^{2+}{}_{(aq)} + CO_2 + \text{surface site}$$

Autocatalytic dissolution with Fe(II)-oxalate complexation

$$Fe^{2+}{}_{(aq)} + C_2O_4{}^{2-} \rightarrow [Fe(C_2O_4)]^{0/2-}{}_{(aq)}$$

Similarly, Al release initially increases due to oxalate chelation, but as stable Al-oxalate complexes form, the release rate decreases.[26,71] Al release remained low across all treatments; OA-1.0 peaked at 1.39 mg g^{-1} and stabilized around 0.55 mg g^{-1} at 360 hours. TSP's Al release declined from 5.68 mg g^{-1} (1 h) to 0.49 mg g^{-1} (360 h).

$$Al^{3+}{}_{(aq)} + 3C_2O_4{}^{2-} \rightarrow [Al(C_2O_4)_3]^{3-}{}_{(aq)}$$

Both Fe and Al release behaviors in OA-ERP are governed by ligand-promoted dissolution mechanisms induced by oxalate. In the case of Fe, oxalate not only chelates Fe^{3+} but also acts as a mild reducing agent, generating soluble Fe^{2+} and Fe(II)-oxalate complexes that facilitate autocatalytic dissolution of hematite surfaces. For Al, oxalate primarily enhances solubility through strong complexation with Al^{3+}, forming highly stable $[Al(C_2O_4)_3]^{3-}$ complexes without redox involvement. Consequently, Fe release involves both surface reduction and complexation, whereas Al release is dominated by ligand exchange and chelation stability, together explaining the characteristic initial burst followed by gradual stabilization observed in Fig. 6(A) and (B).

Quantification of residual oxalic acid (Fig. SI.2) showed values ranging from approximately 295 to 330 mg g^{-1} fertilizer for OA-1.0 and OA-1.2 treatments. These results support the observation of rapid phosphorus release under unbuffered aqueous conditions, where acid dissolution of rock phosphate is expected to dominate.

The phosphate (P) release kinetics of from TSP, OA-0.2 (Fig. 7(A)), OA-0.6 (Fig. 7(B)), OA-1.0 (Fig. 7(D)), and OA-1.2 (Fig. 7(E)) were best fitted by a zero-order model, whereas the control-OA (Fig. 7(F)) and OA-0.9 (Fig. 7(C)) followed a pseudo-first-order model.

In zero-order kinetics, the rate of P release remains constant and is independent of the remaining P concentration within the material. This indicates that release is primarily governed by surface-controlled dissolution, where a fixed amount of phosphate is released per unit time. The steady release observed for TSP and highly oxalate-modified samples (1 : 1 and 1.2 : 1) suggests that oxalic acid treatment effectively enhances $CaHPO_4$ dissolution through acid-mediated reactions and Ca-complexation, maintaining a uniform release profile.

In contrast, the control-O and OA-0.9 followed pseudo-first-order kinetics, where the release rate depends on the remaining concentration of phosphate. This suggests that the release mechanism is likely diffusion-controlled and limited by the gradual dissolution of P from less reactive surfaces.

Overall, the zero-order release behavior of the highly oxalate-modified OA-ERP samples highlights their potential as controlled-release phosphate fertilizers, providing a sustained and predictable supply of available phosphorus over time.

3.3 Soil characterization and soil release study

The Table 3 reviews key physicochemical properties of the tested soil sample. The soil shows a slightly alkaline pH of 7.84 ± 1.01 and a moderate water holding capacity of 20 ± 2.51%. The total phosphorus (P) content is 265.91 ± 41.79 mg kg^{-1}, which falls within the typical soil P range of 0.02% to 0.15% (equivalent to 200–1500 mg kg^{-1}) reported in literature.[72] The total iron (Fe) concentration is 27 511.88 ± 718.27 mg kg^{-1}, aligning with the reported Fe content in agricultural soils (11 058 to 27 721 mg kg^{-1} (ref. 73)). Total aluminium (Al) is relatively low at 89.14 ± 0.31 mg kg^{-1}. In the water-soluble fraction, P and Fe are present at 0.85 ± 0.25 mg kg^{-1} and 7.56 ± 0.003 mg kg^{-1}, respectively, indicating limited mobility. In contrast, water-soluble Al is significantly higher at 10.28 ± 5.87 mg kg^{-1}, suggesting potential solubility and mobility in soil solution.

Fig. 8(A) represents phosphorus (P) release over time from different fertilizer treatments; all applied at a rate of 120 mg P per kg of soil. TSP released phosphorus quickly, exhibiting a rapid spike early on; however, its cumulative release remained relatively low over time, reaching only about 13.6% of the applied P by the 50th day. In contrast, the OA-ERP treatments demonstrated slower but more sustained P release. Among them, OA-ERP with a 0.9 : 1 oxalic acid to ERP ratio was the most effective, releasing over 51.6% of the applied phosphorus by 50 days. The OA-1.0 and OA-1.2 treatments also outperformed both TSP and releasing 22.3% and 28.8% respectively.

Crops such as chilli (*Capsicum annuum*) have substantial P requirements to support optimal growth and fruiting. According to previous studies, most vegetable crops require 25–50 mg of plant-available phosphorus (P) per kg of soil at a given time to maintain adequate fertility, with the critical minimum P level for chilli reported at approximately 15–20 mg P kg^{-1} soil.[74] In the present study, TSP released only ~16 mg P kg^{-1} soil (13.6% of 120 mg kg^{-1} applied) within 55 hours, which is at or slightly below the lower threshold needed to meet chilli's P demand. OA-ERP (0.9 : 1) released ~62 mg P kg^{-1} soil (51.6%) over the same period, surpassing the minimum requirement and providing a more gradual sustained phosphorous supply suitable for continued crop uptake.

This indicates that conventional TSP, despite rapid early release, may not meet the sustained P high P-fixation capacity. Such soils, often rich in iron and aluminum oxides, tend to immobilize added phosphate, reducing its long-term

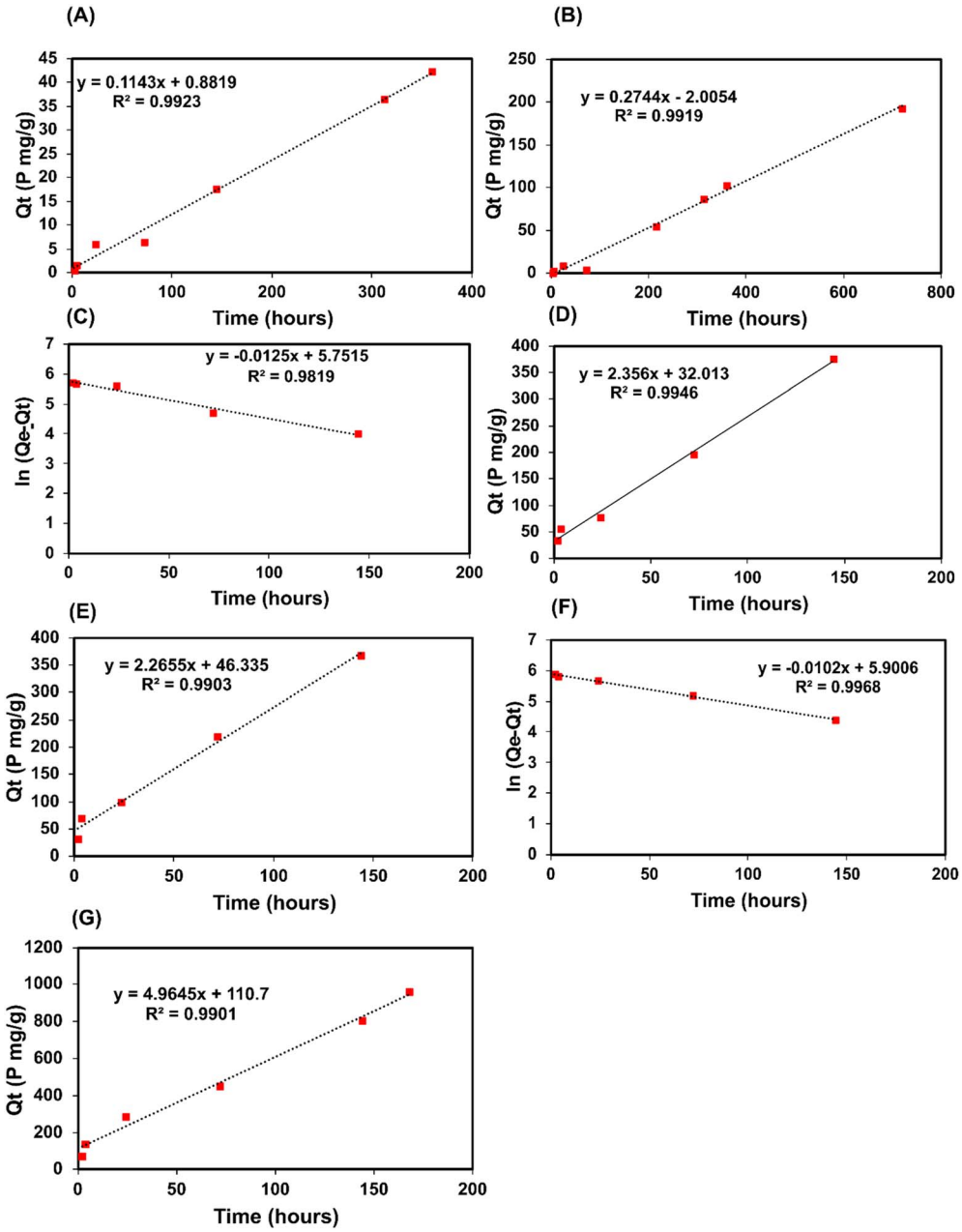

Fig. 7 Fitted kinetics model for P release from OA-ERP samples: (A) OA-0.2 (zero-order), (B) OA-0.6 (zero-order), (C) OA-0.9 (pseudo-first-order), (D) OA-1.0 (zero-order), (E) OA-1.2 (zero-order), (F) control_OA (pseudo-first-order), and (G) TSP (zero-order).

Table 3 Key physicochemical properties of the tested soil sample

Properties	Value
pH	7.84 ± 1.01
Water holding capacity (%)	20 ± 2.51
Bulk density (kg $m^{-3)}$	856.46 ± 10.12
Total P (mg/1 kg soil)	265.91 ± 41.79
Total Fe (mg/1 kg soil)	27 511.88 ± 718.27
Total Al (mg/1 kg soil)	89.14 ± 0.31
Water-soluble P (mg/1 kg soil)	0.85 ± 0.25
Water-soluble Fe (mg/1 kg soil)	7.56 ± 0.003
Water-soluble Al (mg/1 kg soil)	10.28 ± 5.87

availability to plants.[75] Even highly water-soluble fertilizers like TSP frequently fail to maintain adequate soil P levels beyond about three weeks, necessitating repeated applications that increase both cost and environmental risk.[76] In contrast, OA-ERP (0.9 : 1) released approximately four times more P than TSP over the same period, suggesting that comparable or even greater plant-available P could be achieved with roughly half the P input when using the modified ERP.

Fig. 8(B) shows the release of iron (Fe) over time from different phosphorus fertilizer treatments. Initially, at time zero, all treatments released the same amount of Fe (7.56 mg kg^{-1}), likely representing background Fe present in the soil.

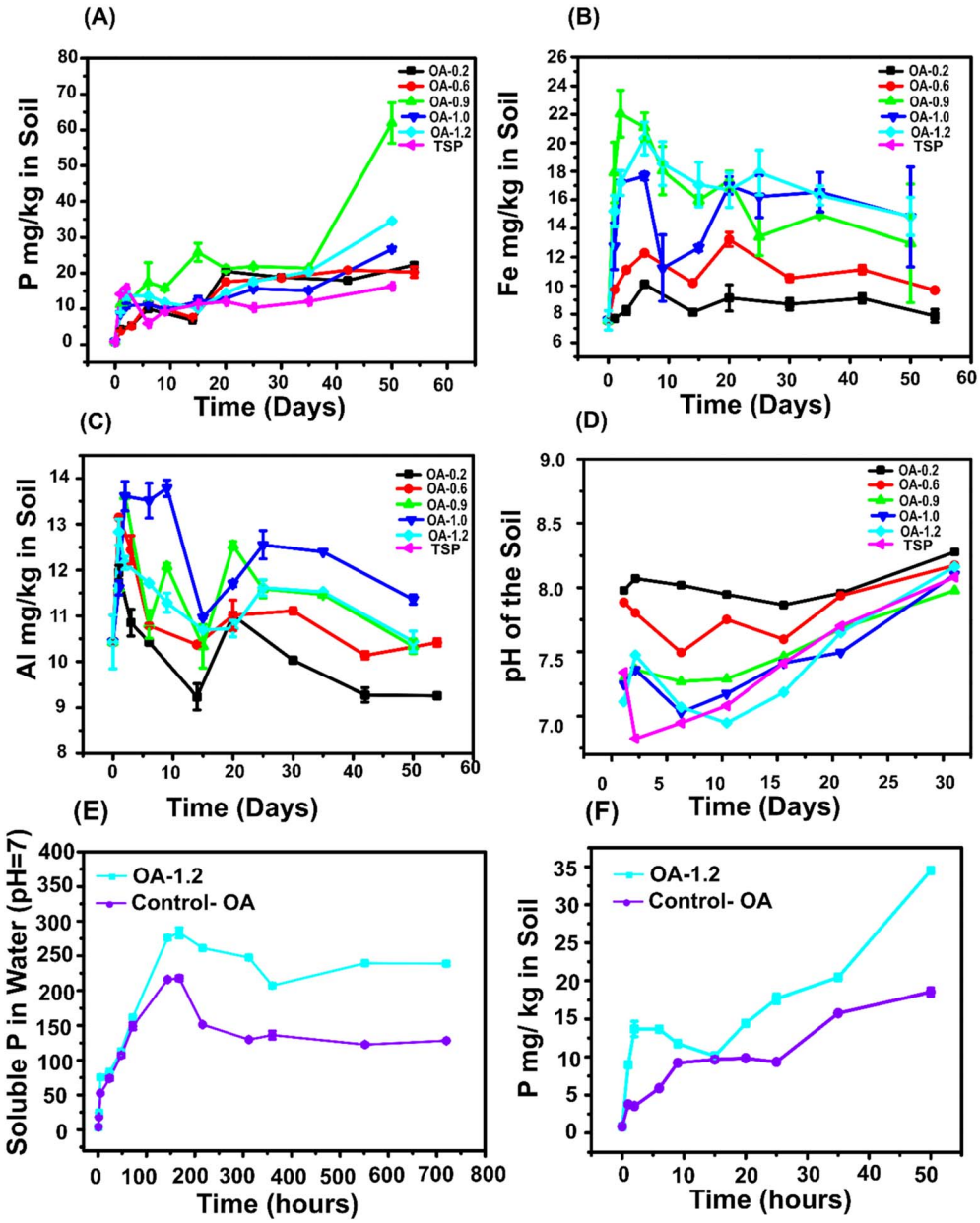

Fig. 8 (A) Phosphorus (P) release from OA-ERP and TSP in soil over time, (B) iron (Fe) release from OA-ERP in soil, (C) aluminum (Al) release from OA-ERP in soil, and (D) variation of soil pH over time following OA-ERP and TSP application ($n = 3$), (E) comparison of phosphorus (P) release over time in water between OA-1.2 and control-OA. (F) Comparison of phosphorus (P) release over time in soil between OA-1.2 and control-OA.

Among the treatments, OA-0.9 exhibited the highest Fe release during the early stages, reaching 22.05 mg kg^{-1} at day 2 and 21.10 mg kg^{-1} at day 6, indicating enhanced Fe solubility and availability. OA-1.2 also showed elevated Fe release, particularly between days 2 and 25, suggesting sustained Fe solubilization over time. Similarly, OA-1.0 maintained moderately high Fe release, comparable to OA-1.2 during the same period. By day 50, Fe levels across all treatments converged to a similar range (11.2–14.8 mg kg^{-1}), indicating a gradual stabilization phase. The Fig. 8(C) shows aluminum (Al) release over time from soil treated with various phosphorus fertilizers, including OA-ERP and control-OA. All treatments stated with the same baseline Al release of approximately 10.29 mg kg^{-1} at time zero, representing the initial water-soluble Al content in the soil. Among the OA treatments, OA-1.0 and OA-1.2 constantly released moderate to high levels of Al, peaking between day 2 and 9. In contrast, OA-0.9 exhibited lower Al release than the other modified ERP treatments, suggesting that this lower ratio may limit Al mobilization while still promoting effective P and Fe release, a potentially beneficial property for reducing soil Al toxicity. Fig. 8(D) shows that soil pH decreased immediately after OA-ERP applying but gradually increased over time. Soil pH remained relatively stable ($\approx$7.0–8.3) across treatments over 30 days, indicating that soil buffering mitigates extreme

acidification. Therefore, while rapid P solubilization occurs in distilled water due to residual acidity, agronomic conditions are better represented by soil-based experiments where controlled nutrient availability is governed by soil–fertilizer interactions rather than simple acid dissolution alone. Although pronounced acidification was observed in unbuffered distilled water, these conditions represent a worst-case scenario. In soil environments, buffering by clay minerals, carbonates, organic matter, and microbial activity is expected to significantly mitigate localized pH reductions.

The same amount of oxalic acid used in OA-1.2 was also applied to a control OA sample without mechanochemical grinding. A small but statistically significant difference ($p < 0.05$) in phosphorus release in water (Fig. 9(A)) and soil (Fig. 9(B)) was observed between OA-1.2 and the control OA, confirming that mechanochemical grinding enhances the reaction between oxalic acid and apatite, improving P release in the final product. This effect can be attributed to the formation of a calcium oxalate coating on apatite surfaces, which acts as a protective layer that inhibits further dissolution,[77] explaining the relatively low solubility observed in the control OA. However, when finer apatite particles (<0.04 mm) were used, the inhibitory effect of the calcium oxalate coating was reduced compared to larger particles (0.2–0.04 mm),[77] likely due to increased surface area and irregularities in the coating. SEM images of OA-1.2 (Fig. 2(E)) support this, showing that mechanochemical grinding reduces particle size and disrupts the crystal structure, thereby limiting the effectiveness of the calcium oxalate barrier. Specifically, SEM images revealed that the OA-1.2 sample exhibited smaller particles, whereas the control-OA (Fig. 2(F)) showed larger, agglomerated, tiny calcium oxalate particles on plate-shaped particles.

3.4 Seed germination bioassay

The phytotoxic and/or phytostimulant potential is assessed by analysing the germination index (GI), which is derived from seed behaviour during germination tests. These tests include parameters such as the relative germination of the seeds (RSG) and the relative growth of the roots (RRG). A new phytostimulant product should be tested before field use, as excessive concentration could inhibit seed germination, plant growth, and affect soil by reducing nitrogen and oxygen, and may contain phytotoxic compounds.[18]

The treatments OA-0.9, OA-1.0, and OA-1.2 were selected for the germination test because they exhibited relatively higher acidity in the water-release study. These levels were therefore chosen to further evaluate their potential toxicity effects. In this experiment, 500 μM extract of OA-ERP, which is equivalent to 100 kg ha^{-1} fertilizer (according to the Sri Lanka DOA standard for TSP for Chilli), was used for the germination test. The relative germination index (RSG%) was calculated by comparing the number of germinated seeds from the extract samples to those germinated in the control sample.[19] The RSG (%) of OA-ERP (Fig. 9(B)) is 151.1%, 143.0%, and 137.5% for OA-0.9, OA-

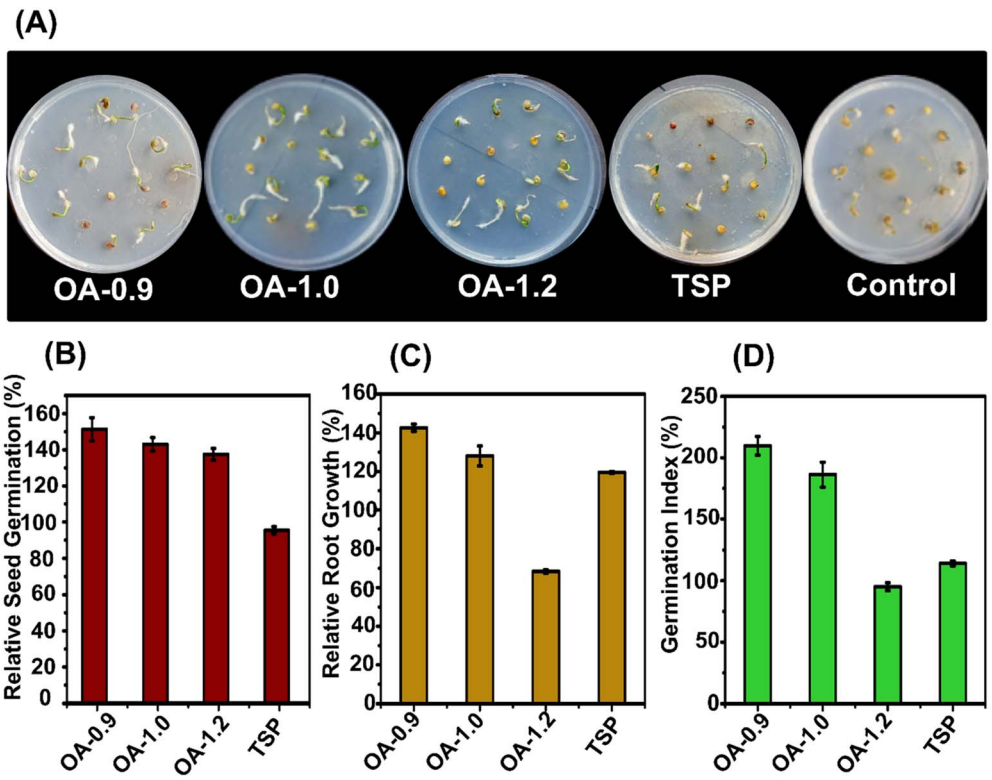

Fig. 9 (A) Seed germination bioassay agar plates incorporating 1 mL of 500 μM phosphorus extract from OA-ERP (OA-0.9, OA-1.0, and OA-1.2) and TSP (control sample-agar media only). (B) Relative seed germination (%) of OA-0.9, OA-1.0, OA-1.2 and TSP (C) relative root growth (%) OA-0.9, OA-1.0, OA-1.2 and TSP (D) germination Index (%) OA-0.9, OA-1.0, OA-1.2 and TSP. ($n = 45$(seeds)).

1.0, and OA-1.2, indicating that OA-ERP stimulates seed germination, likely due to the provision of phosphorus, without indicating aluminium toxicity. These values are substantially higher than those observed in the commercial TSP sample, highlighting the additional advantage conferred by the Fe content in the OA-ERP, which plays a vital role in seed germination. The relative root growth index (RRG%) was calculated by comparing the average length of germinated roots in the extract sample to the control.[19] The RRG % (Fig. 9(C)) of OA-0.9 and OA-1.0 exceeded 100%, indicating a stimulating effect on root development, whereas OA-1.2 registered a value of 68.32%, suggesting moderate toxicity to root growth.

The determination of the germination index (GI) was calculated based on the results of the relative seed germination (RSG) and relative root growth (RRG).[20] According to the literature,[18–21] a (GI) value below 50% indicates high phytotoxicity, while a value between 50% and 80% suggests moderate toxicity. Substances with a GI above 80% are considered non-phytotoxic, and a GI near 0 indicates extreme phytotoxicity. Moreover, a GI exceeding 100% denotes that the extract acts as a highly effective phytonutrient or phytostimulant for the tested seeds.[42] In this study, all samples, including OA-0.9, OA-1.0, OA-1.2, and TSP, exhibit GI values exceeding 80%, thereby confirming their non-toxicity (Fig. 9(D)). Among these, OA-0.9 demonstrates the highest GI value of 209.76%, indicating a phytostimulatory effect at a rate of 100 kg of fertilizer per hectare for chilli seeds.

The observed phytostimulation can likely be attributed to several interacting factors. First, sustained phosphorus (P) availability arises when RP is treated with oxalic acid or other organic acids, enabling the gradual release of phosphate that supports the critical early seedling stage. For example, oxalic-acid-activated phosphate rock significantly increased both

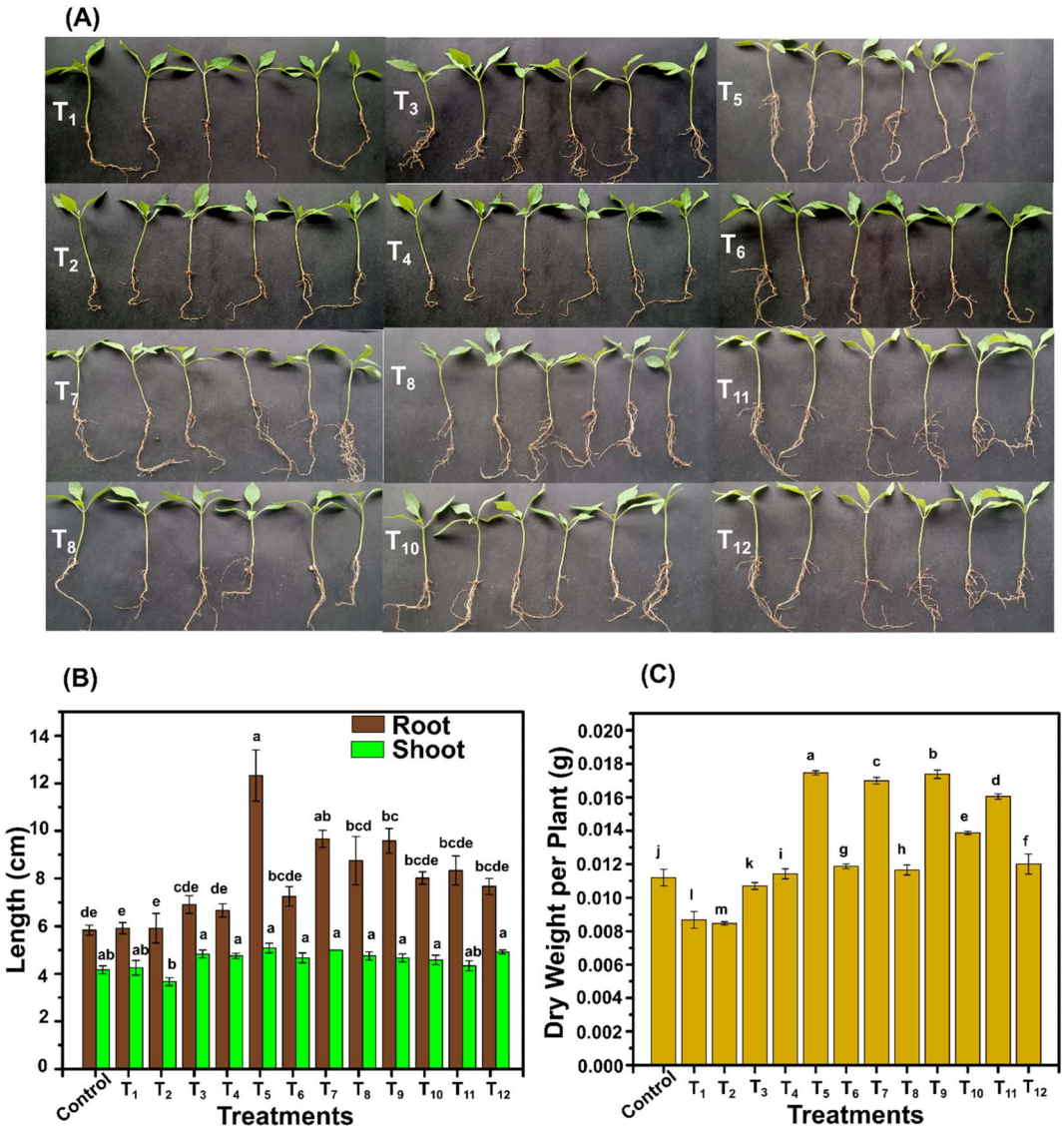

Fig. 10 (A) One-month-old chilli seedlings grown under different phosphorus (P) fertilizer treatments. (B) Root and shoot lengths of seedlings under the various treatments. (C) Dry weight per seedling under different P fertilizer treatments. Different letters indicate statistically significant differences between groups (Tukey's HSD test, $p < 0.05$; $n = 4$).

available soil P and plant uptake in wheat.[78,79] Second, enhanced micronutrient supply may play a role: the treatment can mobilize micronutrients such as Fe^{2+} and Mn^{2+} alongside P, which can contribute additional growth benefits when present at non-toxic levels.[78] Third, organic acid effects such as chelation and root stimulation further support nutrient uptake: the addition of oxalic acid with phosphate rock and phosphate-solubilizing bacteria improved root morphology and biomass in aerobic rice systems.[80] Taken together, these mechanisms suggest that an OA-ERP system serves not only as a controlled-release source of P but also delivers secondary phytostimulatory benefits, *via* chelation, micronutrient mobilization, and root-zone priming. Compared to highly soluble fertilizers such as TSP that provide a rapid but transient P pulse, OA-ERP systems may offer a more sustained and supportive nutrient environment ideal for early-stage crop development.

3.5 Plant growth bioassay

Root length (Fig. 10(B) varied significantly among treatments ($P < 0.05$). T_6 (OA-0.9 at 100 kg ha^{-1}) produced the longest roots at 12.33 ± 1.07 cm, significantly exceeding T_4, T_7, T_8, and T_9 at approximately 9–10 cm. The control treatment showed the shortest roots at 5.88 ± 0.21 cm, while T_1, T_2, T_3, T_5, T_{10}, T_{11}, and T_{12} exhibited intermediate lengths of 7–8 cm. Shoot length (Fig. 10(B)) remained relatively uniform across treatments, ranging from 4 to 5 cm, with no significant differences between most treatments. This indicates that phosphorus availability primarily influenced root development rather than shoot elongation during the seedling stage. T_6 produced significantly longer roots than the control, demonstrating that improved phosphorus nutrition enables robust root development. This root length advantage translates to larger soil exploration volumes and increased nutrient interception, creating positive feedback where enhanced nutrient acquisition further stimulates root growth.[81] The preferential effect on roots *versus* shoots reflects P deficiency's characteristic impact on root development, where plants prioritize photosynthetic capacity over belowground resource acquisition under limitation.[82] Richardson *et al.* (2011)[83] showed that early-established root advantages persist throughout the crop cycle, explaining how seedling vigor in OA treatments translated to superior yield formation. The 100% root length increase in T_6 *versus* the control represents not merely a quantitative but a qualitative transformation in resource acquisition capacity, with more extensive root systems encountering more fertilizer microsites and creating larger rhizosphere volumes, where organic acids and root exudates synergistically mobilize P.

Dry weight per plant (Fig. 10(C) showed significant treatment effects ($P < 0.05$). T_5 (OA-0.9 at 100 kg ha^{-1}) and T_9 (OA-1.2 at 100 kg ha^{-1}) achieved the highest biomass at 0.017 g per plant,

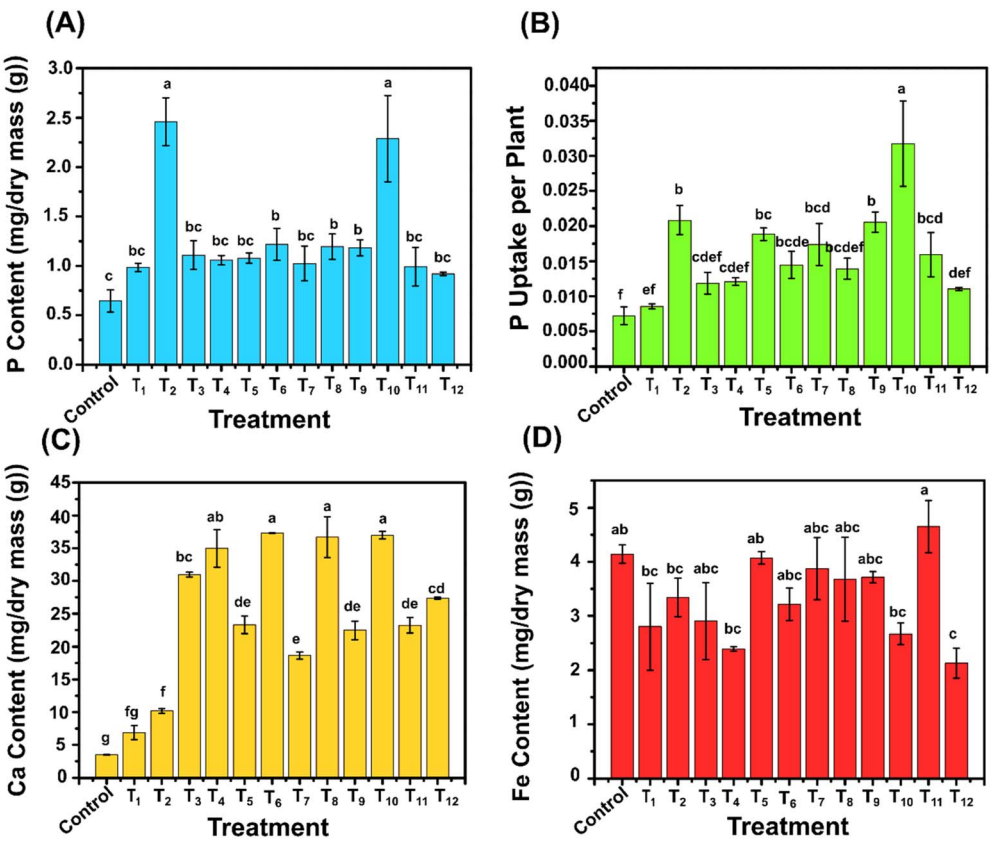

Fig. 11 Effect of different phosphorus fertilizer sources and application rates on early stage chili plant nutrient content. (A) Plant phosphorus content (mg per dry mass, g), (B) phosphorus uptake per plant, (C) Calcium content (mg per dry mass, g), and (D) Iron content (mg per dry mass, g) across different treatments. Different letters indicate statistically significant differences between groups (Tukey's HSD test, $p < 0.05$). ($n = 4$).

followed by T_2, T_6, and T_8 at approximately 0.015–0.016 g per plant. T_1, T_3, T_4, T_7, and T_{10} produced intermediate biomass ranging from 0.011–0.014 g per plant, while the control showed the lowest dry weight at 0.001 g per plant, representing less than half the biomass of the best treatments.

The phosphorus content (Fig. 11(A) differed significantly among treatments ($P < 0.05$). T_2 (OA-0.2 at 50 kg ha^{-1}) and T_{10} (OA-1.2 at 50 kg ha^{-1}) exhibited the highest P content, at 2.46 ± 0.24 mg per dry mass and 2.28 ± 0.43 mg per dry mass, respectively, significantly exceeding the content of all other treatments. T_3, T_4, T_5, T_6, T_7, T_8, T_9, and T_{12} formed an intermediate group with P content of 1.0–1.2 mg per dry mass. T_{11} (TSP 100 kg ha^{-1}) showed a moderate phosphorus (P) content of 0.99 ± 0.19 mg per dry mass, while the control exhibited the lowest P content at 0.64 ± 0.11 mg per dry mass.

P uptake per plant (Fig. 11(B)) showed distinct patterns ($P < 0.05$). T_{10} (OA-1.2 at 50 kg ha^{-1}) demonstrated the highest uptake at 0.031, followed by T_2 at 0.020. T_1, T_3, T_5, T_6, T_7, T_8, and T_9 formed intermediate groups with uptake values ranging from 0.012 to 0.019. T_{11} and T_{12} (TSP treatments) showed moderate uptake at 0.010–0.015, while the control exhibited the lowest uptake at 0.007.

The calcium content (Fig. 11(C)) varied significantly ($P < 0.05$). T_6 (OA-0.9 at 50 kg ha^{-1}), T_8 (OA-1.0 at 50 kg ha^{-1}), and T_{10} (OA 1.2 at 50 kg ha^{-1}) achieved the highest Ca content at approximately 37 mg per dry mass. T_4 and T_9 showed slightly lower values at 23–35 mg per dry mass, while T_1 and T_2 exhibited moderate Ca content at approximately 10 mg per dry mass. The control showed minimal Ca accumulation at 3.4 ± 0.04 mg per dry mass. T_6, T_8, and T_{10} showed significantly higher Ca content than other treatments, reflecting effective dissolution of calcium-phosphate minerals. The variable Ca uptake, despite similar rock phosphate sources, indicates that the OA ratio and application rate influence Ca as well as P availability. However, inverse P–Ca relationships in some treatments suggest competitive uptake mechanisms at root membranes or precipitation reactions in the rhizosphere, temporarily immobilizing both nutrients.[82] White and Broadley (2003)[84] demonstrated that Ca serves essential functions in cell walls, membranes, and signaling, with deficiencies limiting growth even when other nutrients are adequate. The high Ca in top-performing treatments suggests that balanced P–Ca nutrition contributed to superior yields, with both nutrients playing complementary roles in reproductive development. The organic acids in enhanced RP may prevent Ca–P reprecipitation through calcium chelation, maintaining both nutrients in available forms, an advantage over rapid TSP dissolution that creates localized conditions favoring secondary mineral formation.[85,86]

Iron content (Fig. 11(D)) patterns were less consistent ($P < 0.05$). T_{11} (TSP 100 kg ha^{-1}) and the control showed the highest Fe content at approximately 4.5 mg per dry mass. Most OA treatments exhibited moderate Fe levels ranging from 2.5–4.0 mg per dry mass, with T_{12} showing the lowest Fe content at 2.13 ± 0.27 mg per dry mass. The control and T_{11} showed significantly higher Fe content than most OA treatments, presenting an inverse relationship with growth performance.

This paradoxical pattern may reflect Fe–P antagonism where high phosphate concentrations precipitate Fe as ferric phosphate or interfere with Fe translocation within plants.[87] Alternatively, organic acids in enhanced RP treatments may complex Fe, reducing uptake despite potentially mobilizing Fe from soil minerals.[85] The elevated Fe in poorly performing treatments could indicate stress-induced dysregulation of micronutrient homeostasis, where nutritional imbalances disrupt normal uptake controls. Well-nourished plants with adequate P and Ca may utilize Fe more efficiently, requiring lower tissue concentrations to support metabolism. These Fe dynamics emphasize that optimal fertilization must consider complete nutritional balance rather than focusing exclusively on target nutrients, as multi-element interactions substantially influence crop performance.[82]

Correlation analysis revealed significant relationships among measured parameters (Table 4), providing insights into the physiological mechanisms underlying treatment effects. Root length showed strong positive correlation with shoot length ($r = 0.670$, $P < 0.05$) and very strong correlation with dry mass ($r = 0.865$, $P < 0.01$), demonstrating that root system development strongly influenced overall plant biomass accumulation. This aligns with Lynch and Brown (2001),[81] who established that enhanced root growth increases resource acquisition capacity, creating positive feedback loops where better nutrition supports further growth. The strong root-biomass correlation confirms that the root development advantages observed in OA-enhanced treatments translated directly to superior plant growth and yield formation.

Shoot length showed moderate positive correlation with dry mass ($r = 0.562$, $P < 0.05$), though weaker than the root-biomass relationship, indicating that root development was more closely linked to overall growth than shoot elongation. This pattern

Table 4 Correlation matrix among plant growth and phosphorus-related parameters (Pearson correlation).[a]

Parameter	Root length	Shoot length	P content	Dry Mass	P uptake	P utilization
Root length	1.000					
Shoot length	0.670*	1.000				
P content	−0.124	−0.436	1.000			
Dry Mass	0.865**	0.562*	−0.203	1.000		
P uptake	0.398	0.011	0.778**	0.422*	1.000	
P utilization	0.458	0.511*	0.056	0.335	0.238	1.000

[a] Correlation is significant at the 0.05 level (*), correlation is highly significant at the 0.01 level (**).

reflects phosphorus nutrition's preferential effects on root *versus* shoot development during early growth stages.[82] Interestingly, shoot length showed weak positive correlation with P utilization efficiency ($r = 0.511$, $P < 0.05$), suggesting that shoots of more efficient P utilizers grew more effectively despite similar nutrient concentrations.

P uptake per plant showed strong positive correlation with P content ($r = 0.778$, $P < 0.01$), confirming that treatments enhancing P availability increased both tissue concentrations and total P accumulation. The moderate positive correlation between P uptake and dry mass ($r = 0.422$, $P < 0.05$) demonstrates that enhanced P acquisition translated to improved biomass production, though the relationship was not perfectly linear, suggesting other factors also influenced growth. P uptake showed weak positive correlations with root length ($r = 0.398$) and shoot length ($r = 0.011$), indicating that P acquisition capacity was not simply determined by plant size but reflected complex interactions among root architecture, rhizosphere chemistry, and nutrient availability patterns.[83,88]

Olsen-P in soil (Fig. SI.3) ranged from 1.07 to 6.94 mg P 100 g^{-1} soil, with higher values observed in OA-1.2_F and OA-0.9_F treatments compared to TSP and the control, indicating enhanced plant-available phosphorus release from fertilizer-based treatments under alkaline soil conditions.

3.6 Pot trial

Pod number per plant (Fig. SI.5(A)) differed significantly among treatments ($P < 0.05$). T_5 (OA-0.9 at 100 kg ha^{-1}) produced the highest pod count at 11 pods per plant, significantly exceeding all other treatments. T_3, T_4, T_6, T_7, T_8, T_9, T_{10} and T_{11} formed an intermediate group with 7–8 pods per plant. T_1 and T_2 showed moderate pod numbers at approximately 6–8 pods per plant. The control exhibited the lowest pod number at 2 pods/plant.

Fresh pod weight per plant (Fig. SI.5(B)) showed the most dramatic treatment effects ($P < 0.05$). T_5 (OA-0.9 at 100 kg ha^{-1}) achieved the highest fresh pod weight at 92.24 ± 1.51 g per plant, followed by T_7 (OA-1.0 at 100 kg ha^{-1}) at 83.40 ± 1.61 g per plant. T_{11} produced 78.00 ± 2.41 g per plant, while T_6, T_8, and T_9 showed moderate productivity at 65–75 g per plant. The control exhibited minimal productivity at 5 g per plant, representing a 19-fold difference compared to T_5.

The non-linear response to OA ratios reveals complex dose–response relationships. T_1 (OA-0.2) showed exceptional P content despite the lowest organic acid concentration, demonstrating high efficiency at low OA levels. This aligns with Oburger *et al.* (2011),[10] who found that low concentrations of organic acids effectively mobilize P from sparingly soluble sources. However, T_1 produced only moderate yields, suggesting that initial high P availability did not sustain throughout the reproductive phase. Mid-range ratios (0.6–0.9) showed optimal performance for yield formation, with T_5 (OA-0.9) achieving the highest fresh pod weight and T_6 demonstrating exceptional efficiency at the reduced application rate. The highest ratio (OA-1.2) produced variable results, with T_{10} showing maximum P uptake but moderate yield, indicating possible saturation effects or temporal availability differences. Richardson *et al.* (2009)[88] noted that excessive organic acid concentrations can negatively impact microbial communities or create osmotic stress, potentially explaining the diminishing returns at higher ratios.

The 100 kg ha^{-1} rate consistently outperformed 50 kg ha^{-1} across most treatments, demonstrating classical dose–response behavior. However, T_6 (OA-0.9 at 50 kg ha^{-1}) achieved 79.20% of T_5's yield with half the fertilizer, representing approximately 58.63% higher P use efficiency per kilogram applied. This efficiency reflects P's limited soil mobility, where higher concentrations increase the probability of root-fertilizer contact;[61] however, optimal OA ratios can compensate for lower application rates. Syers *et al.* (2008)[89] emphasized that P fixation by soil minerals reduces efficiency, making higher rates typically necessary, but the organic acid protection mechanism reduces fixation losses. T_6's exceptional efficiency demonstrates that properly formulated OA enhancement can achieve near-maximum productivity at reduced rates, offering substantial economic advantages for resource-limited farmers.[46]

OA-enhanced treatments dramatically outperformed TSP despite the latter's high-water solubility. T_5 produced 92.24 ± 1.51 g fresh pod weight *versus* T_{10}'s 50.56 ± 1.89 g—a 90% yield advantage despite identical P application rates. T_1 and T_{10} achieved significantly higher P content than T_{11}, which had a moderate level, challenging the assumption of water-soluble P superiority. The rapid TSP dissolution creates transiently high P concentrations that exceed plant uptake capacity, leading to fixation or leaching losses before absorption.[63] In contrast, OA-enhanced RP provides gradual, sustained P release better matching temporal crop demand throughout the growing season.[90] This synchronization between supply and demand explains the superior agronomic performance despite different solubility characteristics. Arcand and Schneider (2006)[91] demonstrated that progressive P dissolution from enhanced rock phosphate maintains adequate availability during critical reproductive phases, preventing the deficiencies that limit yield even when early vegetative growth appears satisfactory.

T_5's exceptional performance across seedling biomass and final yield demonstrates strong continuity between early vigor and reproductive success. However, T_5's highest pod number, despite moderate seedling performance, indicates that factors beyond early growth influence yield component determination. The divergence between pod number and individual pod weight suggests stage-specific P demands, where adequate P during flowering supports fruit set (determining pod number) while sustained P during pod filling enables maximum individual pod development.[82] T_5's combination of good pod number and maximum pod weight indicates sustained P availability throughout both reproductive phases. White and Hammond (2008)[92] emphasized that P plays critical roles in energy metabolism supporting pollen development, fertilization, and seed formation, with deficiencies at reproductive stages causing yield losses even if vegetative growth appears adequate. The 19-fold yield difference between T_5 and the control exceeds the 2-fold difference in seedling biomass, demonstrating that P nutrition effects amplify during reproductive development when nutrient demands peak.

4 Conclusions

This study demonstrates that mechanochemical activation with oxalic acid can convert low-grade Eppawala rock phosphate into an efficient controlled-release phosphorus fertilizer. The optimized OA-0.9 formulation achieved 96–99% water-soluble phosphorus through the transformation of hydroxyapatite to monetite, providing sustained nutrient release (51.6% over 50 days) compared with 13.6% for TSP, thereby reducing phosphorus fixation in tropical soils. Enhanced nutrient availability resulted in superior agronomic performance, with chili yields reaching 92.24 g per plant, approximately 90% higher than TSP, and improved phosphorus use efficiency, where a half-rate application maintained 79% of maximum yield while increasing efficiency by 58%. This environmentally benign strategy valorizes domestic phosphate resources through green processing and offers a scalable approach for developing sustainable phosphorus fertilizers. Future work should evaluate long-term soil impacts, multi-crop performance, and field-scale validation under diverse agro-ecological conditions.

Nevertheless, the present study was conducted under controlled laboratory and pot-scale conditions using manual mechanochemical grinding; therefore, the findings should be interpreted as a proof-of-concept demonstration rather than an immediately scalable industrial process. The agronomic evaluation was limited to a single crop species and one soil type, and long-term soil health effects, environmental interactions, and multi-season performance were not assessed. Future work should incorporate buffered release tests and oxalic-acid-only controls to separate acidification effects from true fertilizer performance. The interpretation of release kinetics should consider the evolving pH conditions during dissolution, which may contribute to apparent multiphasic behavior through ongoing chemical reactions and mineral transformations. Therefore, the observed release phases likely reflect both intrinsic material properties and dynamic changes in the release environment. Buffered-condition validation and detailed parameter-based kinetic analysis were beyond the scope of the present study and are recommended for future work. In addition, although residual oxalic acid and release behavior were evaluated under laboratory conditions, further studies are required to understand long-term environmental dynamics and microbial interactions in real field systems. Future research should therefore focus on scale-up using controlled mechanochemical milling systems, optimization of process energy and throughput, validation across diverse crops and agro-ecological regions, and extended field trials to evaluate long-term soil fertility, phosphorus cycling, and environmental sustainability.[93,94]

Author contributions

Sanduni Dabare – conduct experiment, formal analysis of data and writing the manuscript. Imalka Munaweera – conceptualization, funding acquisition, methodology, supervision, writing, review and editing the original draft. Saranga Diyabalanage – supervision for XRF characterization, writing, review, and editing the revised manuscript. All authors have approved the final version of the manuscript.

Conflicts of interest

The authors declare that there is no conflicts of interest.

Data availability

All data supporting the findings of this study are included in the manuscript.

Supplementary information (SI) is available. See DOI: https://doi.org/10.1039/d5ra09011c.

Acknowledgements

Financial support for this study is acknowledged by the University of Sri Jayewardenepura, Sri Lanka, under the research grant number RC/URG/SCI/2024/12 and the Instrument Center in the Faculty of Applied Sciences in the University of Sri Jayewardenepura for their support with the relevant instrumental operation and analyses.

References

1 C. Alewell, B. Ringeval, C. Ballabio, D. A. Robinson, P. Panagos and P. Borrelli, Global phosphorus shortage will be aggravated by soil erosion, *Nat. Commun.*, 2020, **11**, 4546.
2 R. B. Chowdhury, G. A. Moore, A. J. Weatherley and M. Arora, Key sustainability challenges for the global phosphorus resource, their implications for global food security, and options for mitigation, *J. Cleaner Prod.*, 2017, **140**, 945–963.
3 T. Fan, T. Ma, M. Wang, S. Wang, X. Wang and A. Lu, Study on phosphorus release from medium- and low-grade phosphate ore powders by mechanical activation and low molecular weight organic acid activation, *Physicochem. Probl. Miner. Process.*, 2024, **60**, 1–19.
4 C. Dimkpa and R. Pandey, Exploring phosphorus fertilizers and fertilization strategies for improved human and environmental health, *Biol. Fertil. Soils*, 2020, **56**, 299–317.
5 C. E. Nedelciu, K. V. Ragnarsdottir, P. Schlyter and I. Stjernquist, Global phosphorus supply chain dynamics: Assessing regional impact to 2050, *Global Food Secur.*, 2020, **26**, 100426.
6 P. D. Johan, O. H. Ahmed, N. A. Hasbullah, L. Omar, P. Paramisparam, N. H. Hamidi, M. B. Jalloh and A. A. Musah, Phosphorus Sorption following the Application of Charcoal and Sago (Metroxylon sagu) Bark Ash to Acid Soils, *Agronomy*, 2022, **12**, 3020.
7 G. Hettiarachchi, E. Lombi, M. McLaughlin, D. Chittleborough and P. Self, *Density Changes Around Phosphorus Granules and Fluid Bands in a Calcareous Soil*, Soil Science Society of America Journal - SSSAJ, 2006, p. 70.
8 W. Wei, X. Zhang, J. Cui and Z. Wei, Interaction between low molecular weight organic acids and hydroxyapatite with

different degrees of crystallinity, *Colloids Surf., A*, 2011, **392**, 67–75.

9 H. A. Khedr, M. O. Ebraheem, H. A. Alshwyeh, N. F. Gumaah, S. R. Al-Mhyawi, A. H. Ragab and A. M. Zayed, Nanoscale grinding: Unlocking the nutrient potential of oxidized phosphate rocks for sustainable fertilizer innovation, *PLoS One*, 2025, **20**(5), e0321095.

10 H. A. Khedr, M. O. Ebraheem and A. M. Zayed, Comprehensive insights into phosphorus solubility and organic matter's impact on black phosphate leaching, *Sci. Rep.*, 2024, **14**(1), 19159.

11 N. Fang, Y. Shi, Z. Chen, X. Sun, L. Zhang and Y. Yi, Effect of mechanochemical activation of natural phosphorite structure as well as phosphorus solubility, *PLoS One*, 2019, **14**(11), e0224423.

12 P. Anastas and N. Eghbali, Green chemistry: principles and practice, *Chem. Soc. Rev.*, 2010, **39**, 301–312.

13 E. D. Roy, Phosphorus recovery and recycling with ecological engineering: A review, *Ecol. Eng.*, 2017, **98**, 213–227.

14 P. J. Withers, M. Rodrigues, A. Soltangheisi, T. S. De Carvalho, L. R. Guilherme, V. d. M. Benites, L. C. Gatiboni, D. M. De Sousa, R. d. S. Nunes and C. A. Rosolem, Transitions to sustainable management of phosphorus in Brazilian agriculture, *Sci. Rep.*, 2018, **8**, 1–13.

15 P. J. Withers, R. Sylvester-Bradley, D. L. Jones, J. R. Healey and P. J. Talboys, Feed the crop not the soil: rethinking phosphorus management in the food chain, *Environ. Sci. Technol.*, 2014, **48**, 6523–6530.

16 P. G. de Souza, J. A. Pallone, E. A. Orlando, A. C. Costa-Santos, E. M. Ayres, A. Rosenthal and A. J. Teodoro, Evaluation of oxalic acid extraction and quantification methods in the different purslane (*Portulaca oleracea* L.) matrices and spinach (*Spinacea oleracea*), *MethodsX*, 2024, **13**, 102863.

17 J. M. Martínez-Vidaurre, E. P. Pérez-Álvarez, E. García-Escudero, M. C. Ramos and F. Peregrina, Differences in Soil Water Holding Capacity and Available Soil Water along Growing Cycle Can Explain Differences in Vigour, Yield, and Quality of Must and Wine in the DOCa Rioja, *Horticulturae*, 2024, **10**, 320.

18 S. Cristea, M.-D. Niculescu, A. Perisoara, E. Ivan, M. Stanca, C.-A. Alexe, B.-M. Tihauan and L. Olariu, Germination Study of Some Protein-Based Gels Obtained from By-Products from the Leather Industry on Tomato and Pepper Seeds, *Gels*, 2024, **10**, 75.

19 N. Pampuro, C. Bisaglia, E. Romano, M. Brambilla, E. Foppa Pedretti and E. Cavallo, Phytotoxicity and Chemical Characterization of Compost Derived from Pig Slurry Solid Fraction for Organic Pellet Production, *Agriculture*, 2017, **7**, 94.

20 T. H. Kebrom, S. Woldesenbet, H. K. Bayabil, M. Garcia, M. Gao, P. Ampim, R. Awal and A. Fares, Evaluation of phytotoxicity of three organic amendments to collard greens using the seed germination bioassay, *Environ. Sci. Pollut. Res.*, 2019, **26**, 5454–5462.

21 Z. Lončarić, V. Galić, F. Nemet, K. Perić, L. Galić, P. Ragályi, N. Uzinger and M. Rékási, The Evaluation of Compost Maturity and Ammonium Toxicity Using Different Plant Species in a Germination Test, *Agronomy*, 2024, **14**, 2636.

22 T. H. Hansen, K. H. Laursen, D. P. Persson, P. Pedas, S. Husted and J. K. Schjoerring, Micro-scaled high-throughput digestion of plant tissue samples for multi-elemental analysis, *Plant Methods*, 2009, **5**, 12.

23 D. Wieczorek, B. Żyszka-Haberecht, A. Kafka and J. Lipok, Determination of phosphorus compounds in plant tissues: from colourimetry to advanced instrumental analytical chemistry, *Plant Methods*, 2022, **18**, 22.

24 M. Motsara and R. N. Roy, *Guide to Laboratory Establishment for Plant Nutrient Analysis*, 2008, vol. 19, pp. 101–122.

25 G. d. O. Mendes, H. M. Murta, R. V. Valadares, W. B. d. Silveira, I. R. d. Silva and M. D. Costa, Oxalic acid is more efficient than sulfuric acid for rock phosphate solubilization, *Miner. Eng.*, 2020, **155**, 106458.

26 Z. Zhang, G. Guo, M. Wang, J. Zhang, Z. Wang, F. Li and H. Chen, Enhanced stabilization of Pb, Zn, and Cd in contaminated soils using oxalic acid-activated phosphate rocks, *Environ. Sci. Pollut. Res.*, 2018, **25**, 2861–2868.

27 G. M. Poralan, J. E. Gambe, E. M. Alcantara and R. M. Vequizo, X-ray diffraction and infrared spectroscopy analyses on the crystallinity of engineered biological hydroxyapatite for medical application, *IOP Conf. Ser.:Mater. Sci. Eng.*, 2015, **79**, 012028.

28 I. Cacciotti, in *Handbook of Bioceramics and Biocomposites*, ed. I. V. Antoniac, Springer International Publishing, Cham, 2016, pp. 145–211, DOI: 10.1007/978-3-319-12460-5_7.

29 I. Macha, C. Charvillat, S. Cazalbou, D. Grossin, U. Boonyang and B. Ben-Nissan, Comparative study of coral conversion, Part 3: Intermediate products in the first half an hour, *J. Aust. Ceram. Soc.*, 2016, **52**, 177–182.

30 M. V. Chaikina, N. V. Bulina, O. B. Vinokurova, K. B. Gerasimov, I. Y. Prosanov, N. B. Kompankov, O. B. Lapina, E. S. Papulovskiy, A. V. Ishchenko and S. V. Makarova, Possibilities of Mechanochemical Synthesis of Apatites with Different Ca/P Ratios, *Ceramics*, 2022, **5**, 404–422.

31 S. V. Dorozhkin, Dissolution mechanism of calcium apatites in acids: A review of literature, *World J. Methodol.*, 2012, **2**, 1.

32 S. Jinawath, D. Pongkao, W. Suchanek and M. Yoshimura, Hydrothermal synthesis of monetite and hydroxyapatite from monocalcium phosphate monohydrate, *Int. J. Inorg. Mater.*, 2001, **3**, 997–1001.

33 S. V. Dorozhkin, Calcium orthophosphates: occurrence, properties, biomineralization, pathological calcification and biomimetic applications, *Biomatter*, 2011, **1**, 121–164.

34 M. Furko and C. Balázsi, Calcium phosphate based bioactive ceramic layers on implant materials preparation, properties, and biological performance, *Coatings*, 2020, **10**, 823.

35 K. Nakamoto, *Infrared and Raman Spectra of Inorganic and Coordination Compounds, Part B: Applications in Coordination, Organometallic, and Bioinorganic Chemistry*, John Wiley & Sons, 2009.

36 A. Balamurugan, S. Rajeswari, G. Balossier, A. Rebelo and J. Ferreira, Corrosion aspects of metallic implants—An overview, *Mater. Corros.*, 2008, **59**, 855–869.

37 R. Z. LeGeros, Properties of osteoconductive biomaterials: calcium phosphates, *Clin. Orthop. Relat. Res.*, 2002, **395**, 81–98.
38 R. Maharana, A. Basu, N. K. Dhal and T. Adak, Biosolubilization of rock phosphate by Pleurotus ostreatus with brewery sludge and its effect on the growth of maize (*Zea mays* L.), *J. Plant Nutr.*, 2021, **44**, 395–410.
39 J. Vekeman, J. Torres, C. E. David, E. Van de Perre, K. M. Wissing, E. Letavernier, D. Bazin, M. Daudon, A. Pozdzik and F. Tielens, In search of an efficient complexing agent for oxalates and phosphates: A quantum chemical study, *Nanomaterials*, 2021, **11**, 1763.
40 A. A. Nayl, W. A. A. Arafa, A. I. Abd-Elhamid and R. A. Elkhashab, Studying and spectral characterization for the separation of lanthanides from phosphate ore by organic and inorganic acids, *J. Mater. Res. Technol.*, 2020, **9**, 10276–10290.
41 B. G. Sukhov, D. Enkhtuyaa, Z. Amgalan, T. I. Vakul'skaya, L. N. Novikova, Z. G. Bazarova and B. G. Bazarov, Effect of mechanical activation on structural-chemical properties of phosphorites, *Russ. J. Appl. Chem.*, 2007, **80**, 853–859.
42 I. Ali, C. Peng, D. Lin, D. Saroj, I. Naz, Z. Mahmood Khan, M. Sultan and M. Ali, Encapsulated green magnetic nanoparticles for the removal of toxic Pb^{2+} and Cd^{2+} from water: Development, characterization and application, *J. Environ. Manage.*, 2019, **234**, 273–289.
43 U. A. J. Ratnayake, K. D. N. Weerasinghe, U. W. A. Vitharana and K. K. J. Chandika, Potential of Eppawala Rock Phosphate as a Phosphorus Fertilizer for Rice Cultivation in Acid Sulphate Soils in Matara District of Sri Lanka, *Trop. Agric.*, 2018, **29**, 293–299.
44 N. Batapola, N. Ratnayake, B. Abeysinghe, R. Premasiri, N. Dushyantha, I. M. S. K. Ilankoon, R. Chandrajith, S. Rohitha, K. Dissanayake, P. Dharmaratne, A. S. Ratnayake and P. Dilshara, The potential of REEs in the Eppawala Phosphate Deposit, Sri Lanka: REE enrichment, mineralization, and economic significance, *Environ. Earth Sci.*, 2023, **82**, 446.
45 A. Pitawala, M. Schidlowski, K. Dahanayake and W. Hofmeister, Geochemical and petrological characteristics of Eppawala phosphate deposits, Sri Lanka, *Miner. Deposita*, 2003, **38**, 505–515.
46 S. S. S. Rajan and J. H. Watkinson, Unacidulated and Partially acidulated phosphate rock: Agronomic effectiveness and the rates of dissolution of phosphate rock, *Fertilizer Res.*, 1992, **33**, 267–277.
47 S. Gypser, *Identification of Phosphate Adsorption Mechanisms on Fe- and Al-Hydroxides and the Influence of Inorganic and Organic Compounds to Reduce Long-Term Phosphorus Fixation on Mineral Surfaces*, 2020.
48 J. J. Mortvedt, R. H. Follett and L. S. Murphy, *Fertilizer Technology and Application*, Meister Publishing Company, 1999.
49 C. Mosimann, T. Oberhänsli, D. Ziegler, D. Nassal, E. Kandeler, T. Boller, P. Mäder and C. Thonar, Tracing of Two Pseudomonas Strains in the Root and Rhizoplane of Maize, as Related to Their Plant Growth-Promoting Effect in Contrasting Soils, *Front. Microbiol.*, 2017, **7**, 2150.
50 D. Zúñiga-Silgado, J. C. Rivera-Leyva, J. J. Coleman, A. Sánchez-Reyez, S. Valencia-Díaz, M. Serrano, L. E. de-Bashan and J. L. Folch-Mallol, Soil Type Affects Organic Acid Production and Phosphorus Solubilization Efficiency Mediated by Several Native Fungal Strains from Mexico, *Microorganisms*, 2020, **8**, 1337.
51 J. Christoffersen, M. R. Christoffersen, W. Kibalczyc and F. A. Andersen, A contribution to the understanding of the formation of calcium phosphates, *J. Cryst. Growth*, 1989, **94**, 767–777.
52 E. Valsami-Jones, K. Ragnarsdottir, A. Putnis, D. Bosbach, A. Kemp and G. Cressey, The dissolution of apatite in the presence of aqueous metal cations at pH 2–7, *Chem. Geol.*, 1998, **151**, 215–233.
53 Y. Raiymbekov, P. Abdurazova and U. Nazarbek, Dissolution Kinetics of Carbonates in Low-Grade Microgranular Phosphate Ore Using Organic Acids as Leaching Agents, *Mining*, 2024, **4**, 766–776.
54 S. Liang, H. Chen, X. Zeng, Z. Li, W. Yu, K. Xiao, J. Hu, H. Hou, B. Liu, S. Tao and J. Yang, A comparison between sulfuric acid and oxalic acid leaching with subsequent purification and precipitation for phosphorus recovery from sewage sludge incineration ash, *Water Res.*, 2019, **159**, 242–251.
55 W. E. Brown, J. P. Smith, J. R. Lehr and A. W. Frazier, Octacalcium phosphate and hydroxyapatite: crystallographic and chemical relations between octacalcium phosphate and hydroxyapatite, *Nature*, 1962, **196**, 1050–1055.
56 J. O. Nriagu, Phosphate–clay mineral relations in soils and sediments, *Can. J. Earth Sci.*, 1976, **13**, 717–736.
57 E. D. Eanes, in *Calcium Phosphates in Biological and Industrial Systems*, Springer, 1998, pp. 21–39.
58 W. Stumm and J. J. Morgan, *quatic chemistry: chemical Equilibria and rates in natural waters {environmental science and technology}*, Wiley, 1996.
59 G. Sposito, *The Chemistry of Soils*, Oxford university press, 2008.
60 D. A. Dzombak and F. M. Morel, *Surface Complexation Modeling: Hydrous Ferric Oxide*, John Wiley & Sons, 1991.
61 M. Hedley and M. McLaughlin, in *Phosphorus: Agriculture and the Environment*, 2005, pp. 181–252, DOI: 10.2134/agronmonogr46.c7.
62 A. P. B. Teles, M. Rodrigues and P. S. Pavinato, Solubility and Efficiency of Rock Phosphate Fertilizers Partially Acidulated with Zeolite and Pillared Clay as Additives, *Agronomy*, 2020, **10**, 918.
63 S. H. Chien, L. I. Prochnow, S. Tu and C. S. Snyder, Agronomic and environmental aspects of phosphate fertilizers varying in source and solubility: an update review, *Nutr. Cycling Agroecosyst.*, 2011, **89**, 229–255.
64 J. Hagin, S. S. S. Rajan, M. K. Boyes and M. Upsdell, Partially acidulated phosphate rocks: Phosphorus release characteristics, *Fertilizer Res.*, 1990, **22**, 109–117.

65 R. N. Roy, A. Finck, G. J. Blair and H. L. S. Tandon, Plant Nutrition for Food Security: A Guide for Integrated Nutrient Management, *FAO Fertilizer and Plant Nutrition Bulletin 16. Food & Agriculture Organization of the United Nations*, Rome, 2006.

66 B. Singla Just, P. M. Binder, N. Guerra-Gorostegi, L. Díaz-Guerra, R. Vilaplana, N. Frison, E. Meers, L. Llenas and A. Robles Aguilar, Phosphorus Release Dynamics from Ashes during a Soil Incubation Study: Effect of Feedstock Characteristics and Combustion Conditions, *Agronomy*, 2024, **14**, 935.

67 C. Du, J.-m. Zhou and A. Shaviv, Release Characteristics of Nutrients from Polymer-coated Compound Controlled Release Fertilizers, *J. Polym. Environ.*, 2006, **14**, 223–230.

68 D. Lawrencia, S. K. Wong, D. Y. S. Low, B. H. Goh, J. K. Goh, U. R. Ruktanonchai, A. Soottitantawat, L. H. Lee and S. Y. Tang, Controlled Release Fertilizers: A Review on Coating Materials and Mechanism of Release, *Plants*, 2021, **10**, 238.

69 D. Panias, M. Taxiarchou, I. Douni, I. Paspaliaris and A. Kontopoulos, *Dissolution of Hematite in Acidic Oxalate Solutions: the Effect of Ferrous Ions Addition*, Elsevier, 1996.

70 Y. Liang, J. Liu, J. Jin, Y. Han and Z. Wei, Effects of low-molecular-weight organic acids on the transformation and phosphate retention of iron (hydr) oxides, *Sci. Total Environ.*, 2024, **940**, 173667.

71 A. Violante, M. Ricciardella and M. Pigna, Adsorption of heavy metals on mixed Fe-Al oxides in the absence or presence of organic ligands, *Water, Air, Soil Pollut.*, 2003, **145**, 289–306.

72 A. Balla Kovács, R. Kremper, J. Kátai, I. Vágó, D. Buzetzky, E. M. Kovács, J. Kónya and N. M. Nagy, Characterisation of soil phosphorus forms in the soil-plant system using radioisotopic tracer method, *Plant, Soil Environ.*, 2021, **67**, 367–375.

73 G. Jha, D. Sihi, B. Dari, H. Kaur, M. A. Nocco, A. Ulery and K. Lombard, Rapid and inexpensive assessment of soil total iron using Nix Pro color sensor, *Agric. Environ. Lett.*, 2021, **6**, e20050.

74 J. Wijewardena, presented in part at the Improving Plant Nutrient Management for Better Farmer Livelihoods, Food Security and Environmental Sustainability, *Proceedings of a Regional Workshop, FAO, Regional Office for Asia and the Pacific*, 2005.

75 D. Sirisena and L. D. B. Suriyagoda, Toward sustainable phosphorus management in Sri Lankan rice and vegetable-based cropping systems: A review, *Agric. Nat. Resour.*, 2018, **52**, 9–15.

76 J. Palihakkara, C. P. Attanayake, L. Burkitt and P. Jeyakumar, Phosphorus Release and Transformations in Contrasting Tropical Paddy Soils Under Fertiliser Application, *J. Soil Sci. Plant Nutr.*, 2025, **25**, 4570–4587.

77 M. Nanzyo, Y. Nakamaru and S.-I. Yamasaki, Inhibition of apatite dissolution due to formation of calcium oxalate coating, *Phosphorus Res. Bull.*, 1999, **9**, 17–22.

78 M. Ahmad, A. Ghoneim, S. S. Al-Oud, K. D. Alotaibi and M. Nadeem, Acidulated activation of phosphate rock enhances release, lateral transport and uptake of phosphorus and trace metals upon direct-soil application, *Soil Sci. Plant Nutr.*, 2019, **65**, 183–195.

79 M. L. Dotaniya, S. C. Datta, D. R. Biswas, H. M. Meena and K. Kumar, Production of Oxalic Acid as Influenced by the Application of Organic Residue and Its Effect on Phosphorus Uptake by Wheat (Triticum aestivum L.) in an Inceptisol of North India, *Natl. Acad. Sci. Lett.*, 2014, **37**, 401–405.

80 Q. A. Panhwar, S. Jusop, U. A. Naher, R. Othman and M. I. Razi, Application of Potential Phosphate-Solubilizing Bacteria and Organic Acids on Phosphate Solubilization from Phosphate Rock in Aerobic Rice, *Sci. World J.*, 2013, **2013**, 272409.

81 J. P. Lynch and K. M. Brown, Topsoil foraging–an architectural adaptation of plants to low phosphorus availability, *Plant Soil*, 2001, **237**, 225–237.

82 H. Marschner, *Marschner's Mineral Nutrition of Higher Plants*, Academic press, 2011.

83 A. E. Richardson, J. P. Lynch, P. R. Ryan, E. Delhaize, F. A. Smith, S. E. Smith, P. R. Harvey, M. H. Ryan, E. J. Veneklaas and H. Lambers, Plant and microbial strategies to improve the phosphorus efficiency of agriculture, *Plant Soil*, 2011, **349**, 121–156.

84 P. J. White and M. R. Broadley, Calcium in plants, *Ann. Bot.*, 2003, **92**, 487–511.

85 W. L. Lindsay and A. Schwab, The chemistry of iron in soils and its availability to plants, *J. Plant Nutr.*, 1982, **5**, 821–840.

86 W. L. Lindsay, *Chemical Equilibria in Soils*, 1981.

87 J. Zhu, M. Li and M. Whelan, Phosphorus activators contribute to legacy phosphorus availability in agricultural soils: A review, *Sci. Total Environ.*, 2018, **612**, 522–537.

88 A. E. Richardson, J.-M. Barea, A. M. McNeill and C. Prigent-Combaret, Acquisition of phosphorus and nitrogen in the rhizosphere and plant, *Plant Soil*, 2009, **321**, 305–339.

89 J. K. Syers, A. Johnston and D. Curtin, Efficiency of soil and fertilizer phosphorus use, *FAO Fertilizer and Plant Nutrition Bulletin*, 2008, vol. 18, pp. 5–50.

90 F. Zapata and R. N. Roy, *Use of Phosphate Rocks for Sustainable Agriculture*, 2004.

91 M. M. Arcand and K. D. Schneider, Plant-and microbial-based mechanisms to improve the agronomic effectiveness of phosphate rock: a review, *An. Acad. Bras. Ciênc.*, 2006, **78**, 791–807.

92 P. J. White and J. P. Hammond, in *The Ecophysiology of Plant-Phosphorus Interactions*, Springer, 2008, pp. 51–81.

93 N. Kottegoda, I. Munaweera, A. N. Madusanka, V. Karunaratne, *Compositions for Sustained Release of Agricultural Macronutrients and Process Thereof*, US 8361185, 2013.

94 I. Munaweera and M. L. C. Madhusha, *Characterization Techniques for Nanomaterials*, 1st edn, CRC Press, DOI: 10.1201/9781003354185.